Aerodynamic and Aeroacoustic Characteristics of an Isolated Propeller at Positive and Negative Thrust

Goyal, J.; Sinnige, T.; Avallone, F.; Ferreira, Carlos

DOI
10.2514/6.2021-2187

Publication date
2021

Document Version
Final published version

Published in
AIAA AVIATION 2021 FORUM

AIAA AVIATION Forum
August 2-6, 2021, VIRTUAL EVENT
AIAA AVIATION 2021 FORUM

10.2514/6.2021-2187

Aerodynamic and Aeroacoustic Characteristics of an Isolated Propeller at Positive and Negative Thrust

Jatinder Goyal*, Tomas Sinnige†, Francesco Avallone‡ and Carlos Ferreira§
Delft University of Technology, Delft, 2629 HS, Netherlands

Regenerative propellers offer many potential benefits such as improved maneuverability, reduced landing run, and decreased community noise, besides the potential to reduce energy consumption by recovering energy during descent and landing. Since the blade loading in regenerative mode will be opposite to that in the conventional propulsive mode, the aerodynamic and aeroacoustic performance of the propeller will be markedly different in both modes of operation. This paper analyzes the performance of an isolated propeller at positive and negative thrust using multi-fidelity numerical approach and validation experiments to identify the most relevant flow phenomena and resulting tonal-noise mechanisms. The results show that the low-fidelity BEM model does not perform well in energy-harvesting conditions mainly due to polar data limitations near the stall conditions at negative angles of attack. The study of tonal noise sources reveals that at a given advance ratio, the loading noise depends upon the relative level of thrust and torque noise in the upstream direction of the propeller, whereas it is lower or similar to the propulsive case in the downstream direction.

Nomenclature

B	=	number of propeller blades
c	=	section chord, m
c_o	=	speed of sound in dry air at 15° C, m/s
C_d	=	$D'/q_\infty c$, sectional drag coefficient
C_f	=	τ_w/q_∞, skin-friction coefficient
C_l	=	$L'/q_\infty c$, sectional lift coefficient
C_p	=	$P'/\rho_\infty n^3 D_p^4$, sectional power coefficient
C_P	=	$P/\rho_\infty n^3 D_p^5$, propeller power coefficient
C_q	=	$Q'/\rho_\infty n^2 D_p^4$, sectional torque coefficient
C_t	=	$T'/\rho_\infty n^2 D_p^3$, sectional thrust coefficient
C_T	=	$T/\rho_\infty n^2 D_p^4$, propeller thrust coefficient
C_{d_R}, C_{l_R}	=	sectional drag and lift coefficient after correction for rotational effects
C_{P_t}	=	total-pressure coefficient, $(p_t - p_\infty)/q_\infty$
$C_{d_{NR}}$, $C_{l_{NR}}$	=	sectional drag and lift coefficient without correction for rotational effects
D	=	drag force, N
D_p	=	propeller diameter, m
h_i	=	average cell size of grid i, m
J	=	V_∞/nD_p, propeller advance ratio
L	=	lift force, N
m	=	harmonic of blade passing frequency
M_{tip}	=	$\Omega R/c_o$, tip rotational Mach number
n	=	propeller rotation speed, Hz
OASPL	=	overall sound pressure level, dB
p	=	static pressure, Pa
p_t	=	total pressure, Pa
$p_{i,m}$	=	pressure fluctuations due to source i for mth harmonic, Pa
p_{ref}	=	reference sound pressure, 2×10^{-5} Pa
p_{rms}	=	acoustic pressure fluctuations, Pa
P	=	propeller power, W
P_C	=	$P/\rho_\infty V_\infty^3 D_p^2$, propeller power coefficient based on freestream dynamic pressure
q	=	$\rho V^2/2$, dynamic pressure, Pa
Q	=	torque, Nm
r	=	radial coordinate, m
R	=	propeller radius, m
Re	=	Reynolds number
T	=	propeller thrust, N
T_C	=	$T/\rho_\infty V_\infty^2 D_p^2$, propeller thrust coefficient based on freestream dynamic pressure
$TSSP$	=	$20\log_{10}\left(p_{rms}/(T/D_p^2)\right)$, thrust-specific-sound-pressure-level, dB
U_ϕ	=	estimated discretization uncertainty
V_∞	=	freestream velocity, m/s
V_{eff}	=	sectional effective velocity, m/s
y^+	=	dimensionless wall distance

*PhD candidate, Wind Energy Section, Faculty of Aerospace Engineering, Kluyverweg 1; J.Goyal@tudelft.nl.
†Assistant professor, Flight Performance and Propulsion Section, Faculty of Aerospace Engineering, Kluyverweg 1; T.Sinnige@tudelft.nl. Member AIAA.
‡Assistant professor, Wind Energy Section, Faculty of Aerospace Engineering, Kluyverweg 1; F.Avallone@tudelft.nl.
§Full professor, Wind Energy Section, Faculty of Aerospace Engineering, Kluyverweg 1; C.J.SimaoFerreira@tudelft.nl.

Greek Symbols

α	=	angle of attack, deg	η	=	JC_T/C_P, propeller efficiency
$\beta_{0.7R}$	=	blade pitch angle at 70% of the radius, deg	θ	=	axial directivity angle, deg
ΔC_d	=	$C_{d_R} - C_{d_{NR}}$	ρ	=	air density, kg/m^3
ΔC_l	=	$C_{l_R} - C_{l_{NR}}$	τ_w	=	wall shear stress, Pa
η_{eh}	=	$8P/\rho_\infty \pi D^2 V_\infty^3$, energy-harvesting efficiency	ϕ	=	inflow angle, deg
			Ω	=	$2\pi n$, rotational speed in rad/s

Subscripts

D	=	drag	$+$	=	positive thrust
L	=	lift	$-$	=	negative thrust
Q	=	torque	∞	=	freestream
T	=	thrust	$'$	=	per unit span
V	=	volume or thickness			

I. Introduction

With the advent of electric flight, the design space has opened up for new configurations where increased interaction between the propulsion system and wing can enhance the aerodynamic performance of the aircraft. The improved aerodynamic efficiency can help overcome the limitations of electric architecture, such as the low energy density of batteries. Some examples of such new configurations are: (i) distributed propulsion with tip-mounted propellers to improve the aerodynamic performance, (ii) regenerative propellers to harvest energy and control aircraft during descent, or (iii) combination of both [1]. This paper focuses on the aerodynamic and aeroacoustic characteristics of isolated regenerative propellers.

During the parts of a mission for which, in principle, no power input is required (descent and landing), a propeller can be used to produce negative torque by adjusting blade pitch and rotational speed so that the angles of attack at the blade sections are negative, see Figure 1. As a result, the electric motor acts as a generator and can harvest energy. Propeller design optimization efforts by Pipistrel for a small electric trainer aircraft led to energy savings of 19%, showing the potential of the concept [2]. Moreover, this concept has been successfully implemented for marine applications in the Opal ship [3]. Different investigations of conventional propellers in the regenerative regime have reported energy-harvesting efficiency of about 10% without any optimization for this mode [1, 4]. However, this efficiency is much lower than the efficiency of modern wind turbines (30-50%, varying with the scale). Therefore, it is important to understand the underlying reasons for the low regenerative performance of propellers. Such knowledge will help improve the energy-harvesting efficiency of propellers without degrading the propulsive performance.

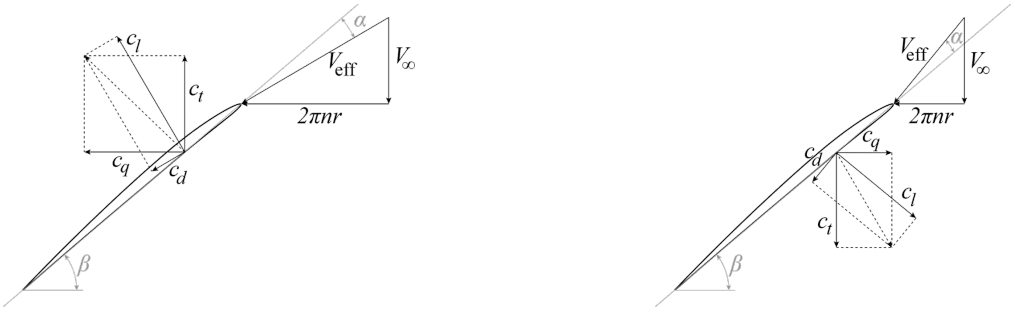

(a) Propulsive mode **(b) Regenerative mode**

Fig. 1 Velocity triangles at a fixed-pitch propeller blade section in propulsive and energy-harvesting mode [1]

Propellers operating at negative thrust settings have been studied in the past for their potential application in decreasing the landing run and increasing the maneuverability. An experimental investigation was done by NACA researchers in 1933 and 1944 to study the effectiveness of the propellers as aerodynamic brake [5, 6]. However, this concept did not gain much attention for a long time. It resurfaced in 1998 when Paul MacCready suggested the use of regenerative propellers in gliders to extend flight time [7]. After that, there have been some studies looking into

the application of regenerative propellers for gliders [8–10]. Until now, the concept has been investigated in detail using analytical, numerical, and experimental methods for turbofans [11–15]. However, the presence of duct and stator in turbofans changes the flow field near the tip of the blade and the mass flow rate compared to unducted single row propellers. Therefore, these results are not directly applicable to unducted rotors, which are of concern in this paper.

In the regenerative mode, a conventional propeller blade with positively cambered airfoils operates near or already separated flow conditions. Therefore, a design modification is required for a conventional propeller to operate efficiently in the regenerative mode without losing the propulsive performance [1]. Generally, low-fidelity tools are required for such design studies due to their low computational costs. One of the most commonly used low-fidelity methods is the blade-element-momentum (BEM) model. However, it is unknown whether the BEM model can be used for accurate performance predictions in the regenerative regime or not. Therefore, an analysis needs to be carried out to check the applicability of BEM in this regime.

The limited literature available on regenerative propellers is focused on aerodynamics, while only a few studies have focused on aeroacoustics. A recent paper [16] studied the effect of windmilling rotors on community noise in which two different landing approaches based on the windmilling drag were investigated by numerically retrofitting a B737-800 aircraft with two hybrid configurations. This study reported a reduction of 4-6 dbA in the noise of the aircraft. However, there is no study (to the best of authors' knowledge) focusing on the noise of unducted regenerative propellers specifically. Understanding the noise generation at the source for such cases is of critical importance due to the lack of acoustic lining around it. As the propeller operates in negative stall or near stall conditions, it could lead to a change in directivity and noise level of the tonal noise compared to the well-known characteristics in the propulsive regime. Moreover, the potential flow separation on the blades could lead to a dominant broadband noise and even structural vibrations and associated structure-borne noise.

In this paper, a detailed investigation has been carried out to check the accuracy of the BEM model in the regenerative regime by comparison against the RANS simulations and the experimental data. Such an analysis is an important step to determine suitability of this low-fidelity tool for the prediction of aerodynamic performance in design optimization studies focused on regenerative performance. Further, the tonal noise characteristics of the regenerative regime have been compared with those occurring in the conventional propulsive regime at a given thrust level and tip rotational Mach number to understand the change in loading noise. For this comparison, the aerodynamic tools - RANS simulations and the classic blade-element-momentum model - have been combined with Hanson's frequency-domain acoustic model [17].

II. Rotor Geometry and Validation Experiments

The analyses discussed in the paper were done with 3-bladed and 6-bladed versions of the same propeller, as shown in Figure 2. The original 6-bladed version is representative of a propeller for a previous-generation regional turboprop aircraft. The propeller blades are unswept, with a propeller diameter of 0.4064 m and a hub diameter of 0.084 m.

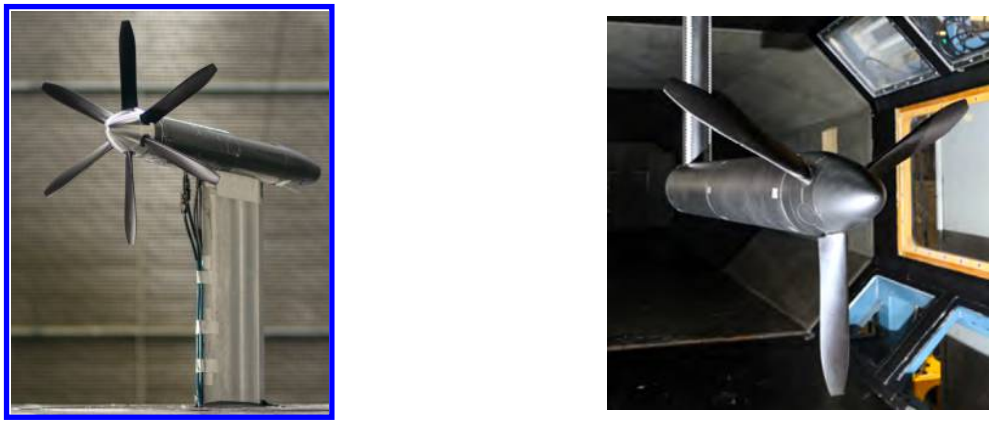

(a) Isolated propeller with six blades installed on a support pylon (propulsive regime).

(b) Isolated propeller with three blades installed on a sting (regenerative regime).

Fig. 2 Propeller geometries considered in this paper [18].

A. Validation Experiments in Propulsive Regime

The validation data for the propulsive part of the operating regime were obtained from wind-tunnel experiments with the six-bladed propeller, see Figure 2a. Three different pitch settings were considered: 20, 30, and 45 deg at 70% radius of the propeller. For the present paper, data were used at a blade pitch setting of 30 deg [19, 20]. The blade geometry is described in Refs. [20] and [21]. The measurements were taken in an open-jet low-speed wind tunnel, with symmetric inflow conditions at a freestream velocity of 30 m/s. The propeller loading was measured with a rotating balance. Details about the experimental procedures are provided in Ref. [21]. The data used in the present paper were not corrected for wind-tunnel boundary interference.

B. Validation Experiments in Regenerative Regime

The investigations focused on the regenerative regime (including propulsive conditions up to moderate thrust coefficients) were done with a three-bladed version of the propeller used for the experiments in the propulsive mode, see Figure 2b. This propeller configuration provides loading conditions more similar to those on general-aviation aircraft. The pitch angle was set to 15 deg at 70% of the radius, as low pitch angles provide better regenerative performance [1]. Only 3 blades were used in order to decrease the absolute level of regenerative power generated, as the dedicated system used to dissipate this power had a limited capacity. Figure 3 shows the test setup inside the wind tunnel.

Fig. 3 Propeller setup for regenerative-propeller experiment installed in Delft University of Technology's Low-Turbulence Tunnel.

The experiments have been described in Ref. [18]. The measurements were taken in the Low-Turbulence Tunnel at Delft University of Technology. This low-speed, closed-return wind tunnel features a closed-wall test section, with a cross-section of 1.80 m × 1.25 m. At the selected freestream velocities, the turbulence level is below 0.1%. A circular support sting was used to mount the propeller model to an external balance, with an integrated turntable to allow for measurements at nonzero angles of attack. The support sting was equipped with zig-zag transition strips to reduce wake blockage. The propeller was driven by an electric motor with customized control hardware and software.

The forces and moments generated by the propeller were measured with an internal six-axis balance integrated into the nacelle of the model. The loading data were complemented by total-pressure measurements in the slipstream of the propeller for selected operating conditions. These data provide insight into the blade loading conditions.

Measurements were taken for sweeps of the propeller advance ratio and angle of attack. The present paper only considers the results measured at 0 deg angle of attack. The advance ratios were set by modifying both freestream velocity and rotational speed of the propeller, aiming to achieve a constant Reynolds number at the blade section at $r/R = 0.7$ of 200,000 for all considered advance ratios. To this end, computations using a blade-element-momentum method were performed before the experiment. The resulting data were used to define a D-optimal test matrix, which

included blocking and randomization to obtain maximum data quality. The advance ratio was varied from 0.5 up to 2.0. The scattered data obtained from the experiment were then used to define polynomial fits to predict the response at any desired advance ratio and angle of attack (within the bounds of the test matrix). Again, the data were not corrected for boundary interference effects. Considering the low thrust coefficients and relatively small rotor area compared to cross sectional area of the test section, such corrections would be negligible for this case.

III. Numerical Methods

A multi-fidelity numerical approach is adopted in this study. This section describes the different models used to simulate the propeller's aerodynamic and aeroacoustic performance.

A. Low-fidelity aerodynamic simulations using blade-element-momentum theory

For the preliminary investigation of the propeller performance, the classic BEM model was implemented based on Refs. [22, 23], and validated using experimental data. The blade section properties (lift and drag polar data) were calculated using RFOIL [24] which is a modification of the well-known 2D-panel method XFOIL [25]. The Reynolds number for the polar data was calculated based on the local effective velocity and chord of the airfoil sections along the blade span. RFOIL was selected because of its better prediction of lift and drag coefficient in the post-stall region [26]. Moreover, RFOIL also provides the option to include the effect of Coriolis and centrifugal forces on the boundary-layer characteristics of rotating airfoils using a quasi-3D model [27, 28]. The present paper includes a discussion of the impact of these corrections on the performance predictions.

The motivation behind the BEM investigations was to evaluate the validity of this model in the regenerative regime (where blade stall is expected) by comparing the results with CFD simulations and experimental data. Due to its low computational cost, BEM can be an important tool for aerodynamic and aeroacoustic design optimization studies focused on improving the performance in negative thrust conditions (without affecting the performance of the propulsive regime). Therefore, it is important to evaluate its applicability in the regenerative regime.

B. CFD simulations with RANS solver

The RANS equations for compressible flow have been solved using ANSYS®Fluent 2019 R3 [29] which is a commercial, unstructured, finite volume, cell-centered solver. As only uniform inflow conditions have been studied in this paper, the simulations have been solved for a single-blade wedge domain in a steady manner using a multi-reference-frame approach. Considering the differences in propeller geometries used for the investigations of the propulsive and regenerative conditions, different domains were used for both cases, shown in Figure 4. Note that the height of the domain in the vicinity of the propeller blade is increased from 1.2R in the 6-bladed configuration to 1.5R in the 3-bladed configuration to allow for wake expansion in the latter case due to negative thrust conditions. Also, the total height of the domain for the 6-bladed configuration is 15R, whereas for the 3-bladed configuration is 10R. As the wedge angle of the latter case (120°) is twice the angle of the former case (60°), the total height of the domain of the latter case was decreased to 10R to reduce the grid size. It was made sure that the boundaries of the domains were sufficiently far away to keep the influence of boundary conditions on the flow properties near the propeller blade minimum [1, 30, 31]. Following the CFD setup of these previous research efforts for similar problems, pressure inlet, pressure outlet, and pressure far-field boundary conditions were used in combination with a conformal periodic boundary condition for the side boundaries to avoid interpolation errors. The propeller blade and spinner were modeled as no-slip walls and the nacelle was modeled as a moving wall to keep it stationary in the absolute frame. The density of air was calculated assuming it to be an ideal gas and the dynamic viscosity was computed using Sutherland's law. The turbulence modeling was based on the Spalart-Allmaras method with a modification proposed by Dacles-Mariani et al. [32, 33].

1. Grid Dependence study

ANSYS Meshing was used for grid generation. Adjacent to no-slip wall regions, a triangular wall mesh was used along with layers of semi-structured prismatic and tetrahedral elements. On the other hand, in the slipstream and upstream of the propeller, an unstructured hexagonal mesh was created to reduce the total number of elements. The first-layer thickness of inflation layers was tuned to keep the $y^+ \leq 1$ as per the requirement of the Spalart-Allmaras turbulence model. The grid density in the whole domain was controlled by wall refinement of no-slip walls and volume refinement of the domains.

For the grid dependence study, the grid was refined systematically, except for the inflation layer as per the

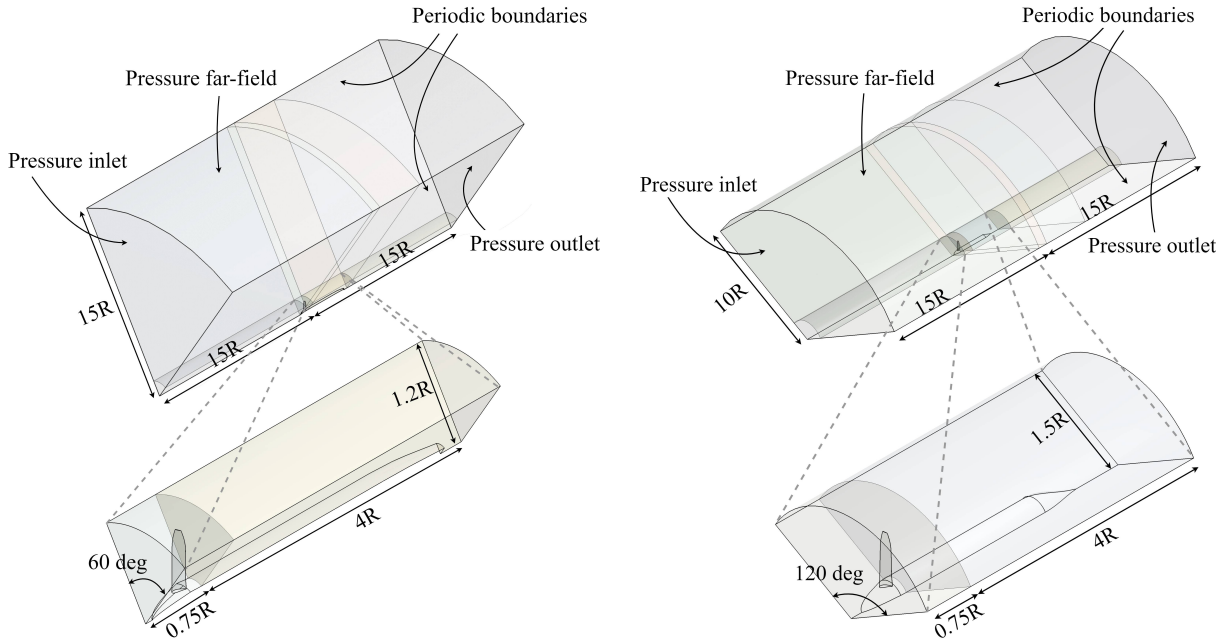

(a) 6-bladed propeller, $\beta_{0.7R} = 30°$ **(b) 3-bladed propeller, $\beta_{0.7R} = 15°$**

Fig. 4 Numerical domain and boundary conditions

recommendation of Roache [34]. Following the methodology of Stokkermans et al. [30], the least-squares version of the grid convergence index proposed by Eça and Hoekstra [35] was used to estimate discretization error. Table 1 lists the grid size and refinement ratios h_i/h_1 for the studied configurations, where h_i is the average cell size of the grid i and h_1 represents the finest grid's average cell size. Note that grid 6 is the coarsest, whereas grid 1 is the finest. Five different grids were used for the mesh dependence study of the 3-bladed propeller, whereas six different grids were used for the 6-bladed propeller configuration. For both configurations, grid 3 was determined to be the most suitable in terms of the tradeoff between computational cost and solution refinement.

Table 1 Grid size of the isolated propeller simulations

	3-bladed		6-bladed	
Grid	Number of cells	h_i/h_1	Number of cells	h_i/h_1
6	– –	– –	2,107,066	1.91
5	3,743,754	1.68	3,098,338	1.68
4	5,299,745	1.49	4,246,837	1.51
3	8,390,961	1.28	7,073,700	1.28
2	11,723,153	1.15	9,586,613	1.15
1	17,644,556	1.00	14,721,611	1.00

The grid-convergence analysis was performed for the thrust and power coefficients for both configurations. The results are given in Table 2 and 3, where U_ϕ represents the estimated discretization error based on the solution of grid 3. Due to the onset of separation in the 3-bladed configuration near the tip of the blade (discussed later in section IV.A.2 in relation to Figure 8), an oscillatory convergence is observed for all the operating points with maximum estimated discretization error of 3.16% and 6.59% for C_T and C_P, respectively. To further check the discrepancies between solutions obtained for different grids, radial distributions of thrust and power are compared in Figure 5 for the operating point corresponding to the maximum uncertainty ($J = 1.00$). It can be observed that except for some small differences in the outer region of the blade due to the onset of separation, the solutions for all the grids are in reasonable agreement.

In contrast, less separation occurred for the 6-bladed, $\beta_{0.7R} = 30°$ configuration, resulting in a lower variation in the C_T and C_P for different grids. The maximum uncertainty for this configuration is about 1% at $J = 0.60$.

From the above study, it was concluded that grid 3 is sufficient for the current analysis compared to the denser grids.

Table 2 Grid dependence study of 3-bladed propeller configuration

	$J = 0.57$		$J = 1.00$		$J = 1.15$		$J = 1.60$	
Grid	C_T	C_P	C_T	C_P	C_T	C_P	C_T	C_P
5	0.04793	0.04065	-0.09322	-0.03279	-0.14237	-0.06437	-0.23322	-0.10346
4	0.04780	0.04068	-0.09334	-0.03303	-0.14263	-0.06476	-0.23475	-0.10512
3	0.04744	0.04074	-0.09350	-0.03304	-0.14287	-0.06483	-0.23331	-0.10368
2	0.04769	0.04069	-0.09252	-0.03232	-0.14168	-0.06389	-0.23330	-0.10366
1	0.04779	0.04076	-0.09295	-0.03281	-0.14240	-0.06462	-0.23420	-0.10440
$\lvert U_\phi \rvert$, %	3.10	0.80	3.16	6.59	2.49	4.36	1.97	4.81

Table 3 Grid dependence study of 6-bladed propeller configuration

	$J = 0.60$		$J = 0.80$		$J = 1.00$		$J = 1.20$	
Grid	C_T	C_P	C_T	C_P	C_T	C_P	C_T	C_P
6	0.32617	0.34029	0.26046	0.30250	0.19011	0.24848	0.10851	0.16842
5	0.32651	0.34039	0.26057	0.30255	0.19025	0.24860	0.10857	0.16843
4	0.32640	0.34015	0.26063	0.30258	0.19018	0.24849	0.10849	0.16833
3	0.32635	0.33994	0.26074	0.30263	0.19018	0.24847	0.10845	0.16827
2	0.32728	0.34081	0.26078	0.30264	0.19013	0.24839	0.10840	0.16821
1	0.32650	0.33966	0.26087	0.30275	0.19027	0.24860	0.10859	0.16846
$\lvert U_\phi \rvert$, %	1.02	1.02	0.20	0.11	0.25	0.26	0.52	0.46

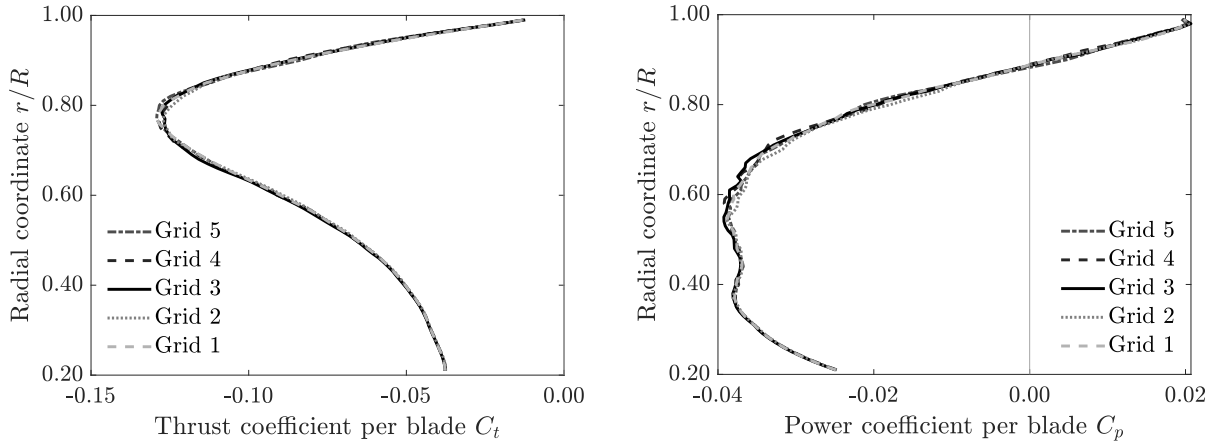

(a) Thrust distribution **(b) Power distribution**

Fig. 5 Effect of mesh refinement on the thrust and power distribution along the propeller blade for the configuration with highest discretization uncertainty (3-bladed, $\beta_{0.7R} = 15°$, $J = 1.00$)

C. Hanson's Tonal Noise Model

There are various analytical models available in the literature based on the Ffowcs Williams and Hawkings (FW-H) formulation to predict the tonal noise of rotors. The models by Gutin [36] and Deming [37], Barry et al. [38], Hanson [17], and Farassat [39] are most commonly used. All of these models require blade loading as input and, therefore, are coupled with BEM or CFD simulations to obtain the propeller tonal noise. The more accurate the blade loading, the more accurate the tonal noise prediction will be. Following the recommendation of Kotwicz et al. [40], Hanson's model was chosen for this research given its capability to handle subsonic as well as supersonic regimes in addition to complex geometries. Though it is unknown if Hanson's model is accurate for cases with significant flow separation, it is considered to be an adequate tool for this study.

For verification of the numerical implementation of the model, the results were compared with test case 5* of Ref. [40]. This case was specifically chosen due to the availability of blade loading in the original study of the propeller by NASA [41]. The results of the implementation showed a good match with the reference study results. In this paper, the blade loading and thickness were assumed to be parabolically distributed along the chord. A sensitivity study has been carried out to evaluate the effect of radial loading distributions obtained from BEM and RANS on the predicted tonal noise. Further, Hanson's model has been coupled with RANS to study the loading noise characteristics of a conventional propeller at a given absolute thrust level in the propulsive and the regenerative regimes.

IV. Results

The propeller performance has been predicted using the BEM and RANS simulations. The numerical methods have been validated using the experimental data (IV.A). The effect of corrections for rotational effects on BEM predictions is evaluated (IV.B). Moreover, the slipstream total pressure coefficients predicted by RANS are compared against the experimental data. The blade loading predicted by the BEM model in the regenerative mode has been compared with the RANS simulations (IV.C). Further, the sensitivity of Hanson's model to the radial distributions provided by BEM and RANS has been evaluated in IV.D. Finally, the tonal noise characteristics of the positive and negative thrust cases have been analyzed at constant freestream and tip rotational Mach number (IV.E).

A. Comparison of BEM and RANS with Experimental Results

In this section, the aerodynamic performance predictions by BEM and RANS are compared with the experimental data to analyze their reliability in the propulsive and the regenerative regimes.

1. Propulsive Regime

The numerical methods (BEM and RANS) have been validated for the propulsive regime by comparing the predictions with the experimental data at V_∞ = 30 m/s, $\beta_{0.7R} = 30°$, see Figure 6. Two different types of results are obtained from the BEM model:

- **NR** - effect of rotation on the blade section characteristics is not considered in the BEM model;
- **R** - effect of rotation on the blade section characteristics is taken into account in the BEM model using the quasi-3D model available in RFOIL.

It is observed that there is a negligible effect of inclusion of rotational effects on the BEM predictions. For the considered operating conditions, the blade sections are not operating close to the stall. Therefore, the impact of the rotational corrections is small because the corrections have the largest impact near stall conditions [27, 28]. The BEM model gives a reasonable qualitative agreement with the experimental data. The offset in thrust and power between the BEM and experiment (Figures 6a and 6b) is most probably due to a difference in turbulence level and transition point on the blade sections between the experiment and numerical simulations, leading to inaccurate lift and drag predictions of blade sections by RFOIL.

The RANS simulations were performed at four different advance ratios as listed in Table 3. They are in excellent agreement with the experimental data for advance ratio up to 1.0. At higher advance ratios, the RANS simulations overpredict the thrust due to underprediction of viscous effects. This results in overprediction of propeller efficiency as compared to the experiment (Figures 6c and 6d). The sudden decrease in efficiency predicted by the experiment at an advance ratio of about 1.2 is due to the strong decrease in profile and span efficiency at low or even negative loading conditions. Similar to the RANS simulations, the BEM model also overpredicts the maximum efficiency and the corresponding advance ratio due to underprediction of viscous effects.

*four-bladed SR2 propeller with freestream Mach number of 0.2 and helical tip Mach number of 0.77

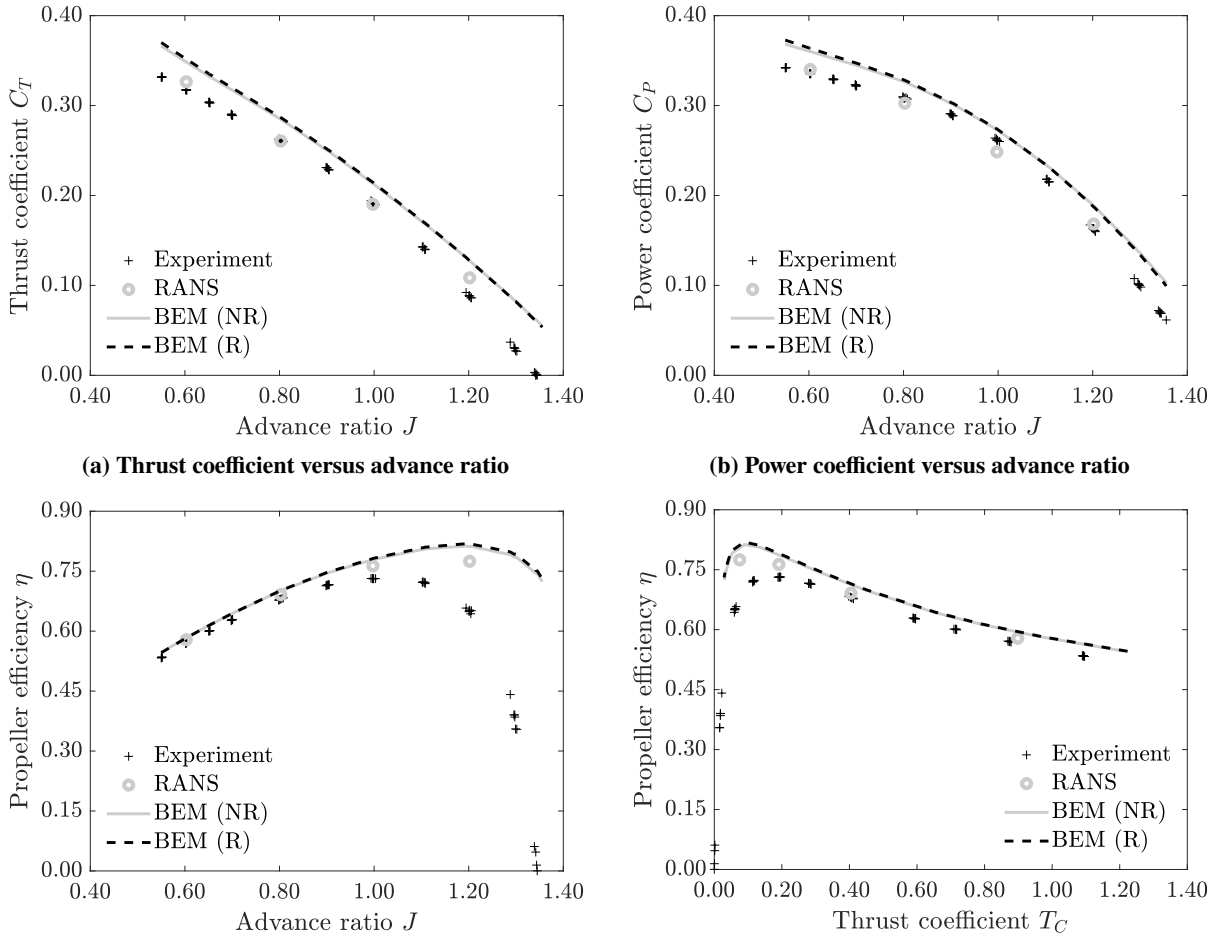

(a) Thrust coefficient versus advance ratio

(b) Power coefficient versus advance ratio

(c) Propeller efficiency versus advance ratio

(d) Propeller efficiency versus thrust coefficient

Fig. 6 Comparison of BEM and RANS predictions with experimental data in propulsive regime (V_∞ = 30 m/s, $\beta_{0.7R}$ = 30°)

2. Regenerative Regime

To evaluate the accuracy of the considered numerical methods in the regenerative regime, the 3-bladed propeller with $\beta_{0.7R} = 15°$ was considered. The comparison of the BEM and RANS predictions with the experimental data is shown in Figure 7. Note that in contrast to the previous case, the inclusion of rotational effects leads to a considerable change in the BEM predictions. Without rotational correction, the BEM predictions start deviating considerably from the experimental data upon entering the regenerative mode, and therefore, cannot be used to reliably predict the regenerative performance of the propeller. The rotational corrections are especially important near and after the stall conditions. Therefore, these corrections are important in the regenerative regime due to the operation of positively cambered airfoils at negative local angles of attack. The BEM model performs much better when the rotational effects on the blade section characteristics are considered. BEM (R) shows a good agreement for thrust coefficient over the whole range of advance ratio (Figure 7a). The prediction of regenerative power is in agreement up to $J = 1.2$, after which there is a large deviation from experimental data, see Figure 7b. The reason for the deviation in C_P is the delayed stall prediction in RFOIL [27, 28] leading to the overprediction of lift and underprediction of drag. As in the regenerative regime, the lift and drag components add up in the thrust force (refer to Appendix A), the overall effect is reduced, whereas both the components subtract for power, leading to an enhanced effect and a large deviation from the experiment. Even though there is a deviation in the predicted energy-harvesting efficiency, the most efficient operating condition predicted by the BEM model (when corrected for rotational effects) lies in the vicinity of the experimental optimal point (Figure 7c). Therefore, the BEM model with rotational corrections can be used to estimate the most optimum operating condition for the given propeller. Similarly, though BEM slightly underpredicts the negative thrust, it can still be used to get a

reasonable estimate, see Figure 7d.

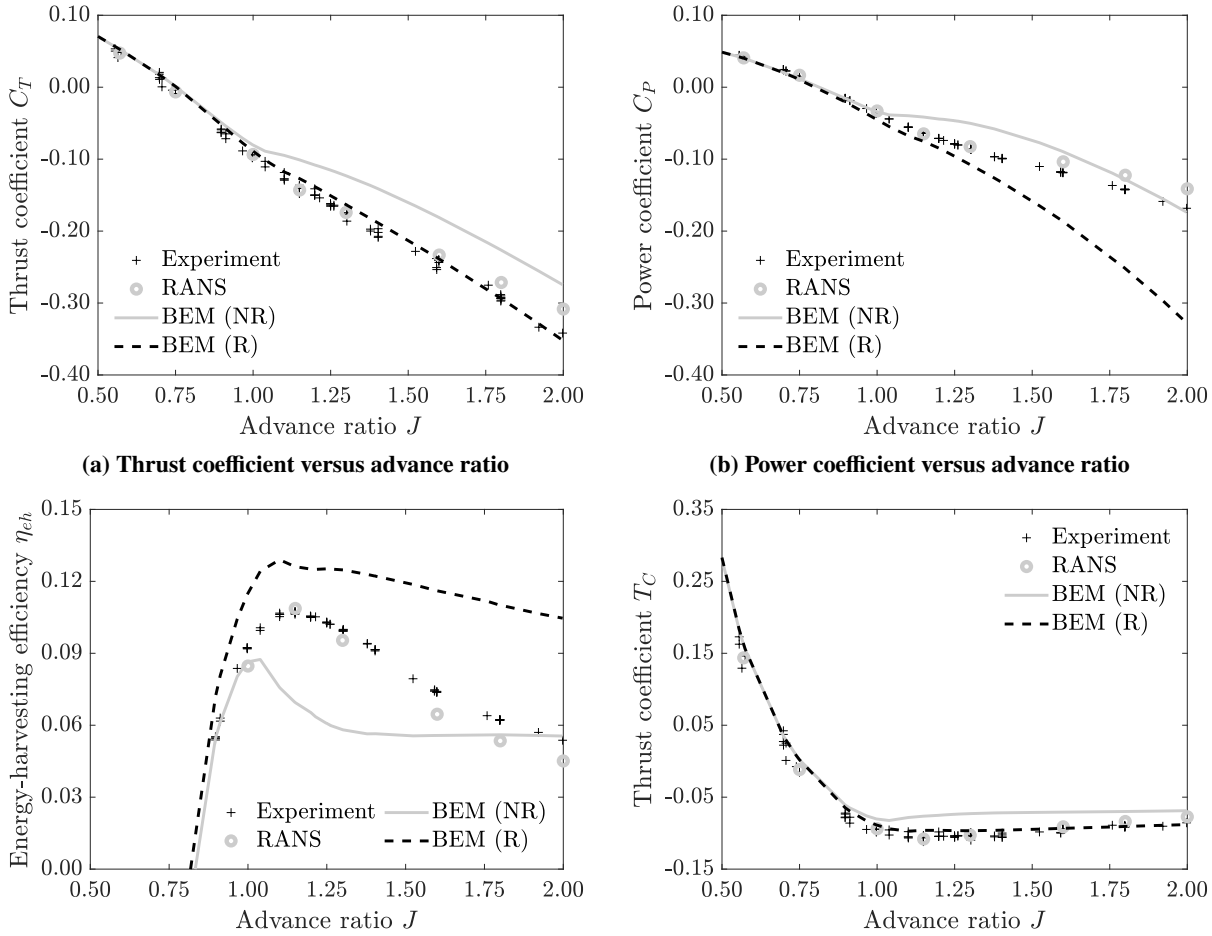

(a) Thrust coefficient versus advance ratio

(b) Power coefficient versus advance ratio

(c) Energy-harvesting efficiency versus advance ratio

(d) Thrust coefficient versus advance ratio

Fig. 7 Comparison of BEM and RANS predictions with experimental data in regenerative regime ($\beta_{0.7R}$ = 15°)

For this configuration, the RANS simulations were performed at eight different operating conditions listed in Table 4. The RANS simulations show a good agreement with the experiment for power and thrust up to an advance ratio of 1.30. However, at higher advance ratios RANS predicts a lower thrust and power compared to the experiment. The reason for the deviation is the stall of the flow along the whole propeller blade at higher advance ratios which is not captured accurately by the RANS simulations.

Table 4 Operating conditions simulated using RANS for the 3-bladed configuration ($\beta_{0.7R}$ = 15°)

J	0.57	0.75	1.00	1.15	1.30	1.60	1.80	2.00
V_∞	23.62	30.13	38.60	43.29	47.62	54.95	58.86	62.46
n	101.16	98.86	95.19	92.67	90.03	84.56	80.50	76.93

Further, to visualize the flow field around the propeller blade, the flow streamlines are plotted at three different blade sections - 0.3R, 0.6R, and 0.9R for four different advance ratios (J = 0.57, 1.00, 1.15, and 1.60) in Figure 8. Also, the distribution of skin friction and the shearlines are shown along with the direction of local shear stress as obtained from the RANS simulations. In Figure 8a, there is an onset of a leading-edge separation bubble on the outboard part of the blade in the propulsive condition due to negative angles of attack faced by the positively cambered blade sections at

$J = 0.57$. Clearly, the selected blade pitch angle is not optimal for the propulsive mode. As the rotational speed of the propeller is reduced to operate in the regenerative mode, the angles of attack faced by the blade sections become even more negative (refer to Figure 1b), resulting in stall of the propeller blades. The stalled region grows from the outboard part towards the inboard part of the blade with the increase in advance ratio. In contrast to the outboard thin airfoils, the thick airfoils at the root exhibit trailing edge separation, see Figures 8b and 8c. The operating condition $J = 1.15$ corresponds to the most efficient energy-harvesting condition (Figure 7), at which only a small inboard part of the blade has attached flow. Therefore, there is a definite potential to improve the regenerative efficiency by improving the flow attachment over the blade span. However, this should not come at the cost of reduced performance in the propulsive regime. At $J = 1.60$, the propeller blade is completely stalled (Figure 8d). The observation of flow separation in regenerative mode is consistent with the previous study discussed in Ref. [1]. Due to the inability of steady RANS to model stalled flowfields accurately [42, 43], there is a deviation between RANS and experiment at high advance ratios.

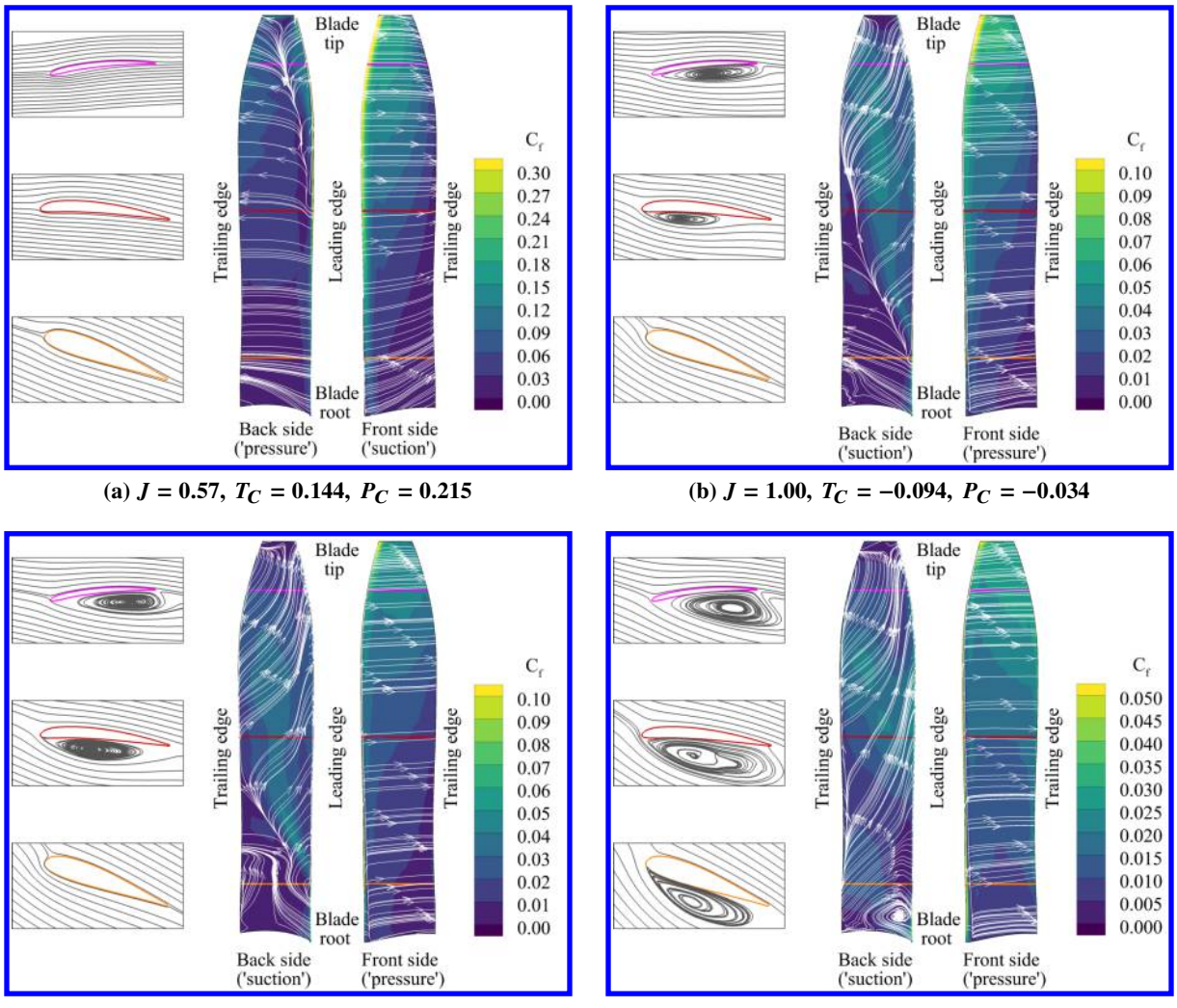

(a) $J = 0.57$, $T_C = 0.144$, $P_C = 0.215$ **(b) $J = 1.00$, $T_C = -0.094$, $P_C = -0.034$**

(c) $J = 1.15$, $T_C = -0.108$, $P_C = -0.043$ **(d) $J = 1.60$, $T_C = -0.093$, $P_C = -0.025$**

Fig. 8 Visualization of flow around propeller blades using skin friction coefficient and shear lines (CFD data)

B. Rotational Effects

Another interesting phenomenon that can be noticed in Figure 8 is the radial outboard pumping of the flow when the flow is separated or about to separate. The centrifugal force pushes the flow in stagnant regions towards the tip that results in a Coriolis force and acts as a favorable pressure gradient, delaying the stall, resulting in higher lift coefficients compared to a non-rotating blade. This phenomenon is known as the Himmelskamp effect [44]. This effect can be

clearly seen in the inboard part of the blade in Figure 8b and Figure 8c. This effect is the so-called "rotational effect" mentioned earlier in this paper. As evident, it is an important phenomenon affecting the regenerative performance of the propeller. Therefore, it becomes important to include these effects while calculating the blade section characteristics. When this effect is not considered, the BEM model predicts worse performance in the regenerative regime than the experiment, see Figure 7. Therefore, it can be concluded that when the blade sections are operating at high angles of attack (negative or positive), the correction for rotational forces becomes important. As mentioned earlier, RFOIL uses a quasi-3D model to account for this effect. The effect of the rotational correction on the blade section characteristics is shown in Figure 9. The effect of the correction is more prominent near the root and decreases towards the tip of the blade, which is as expected from theory.

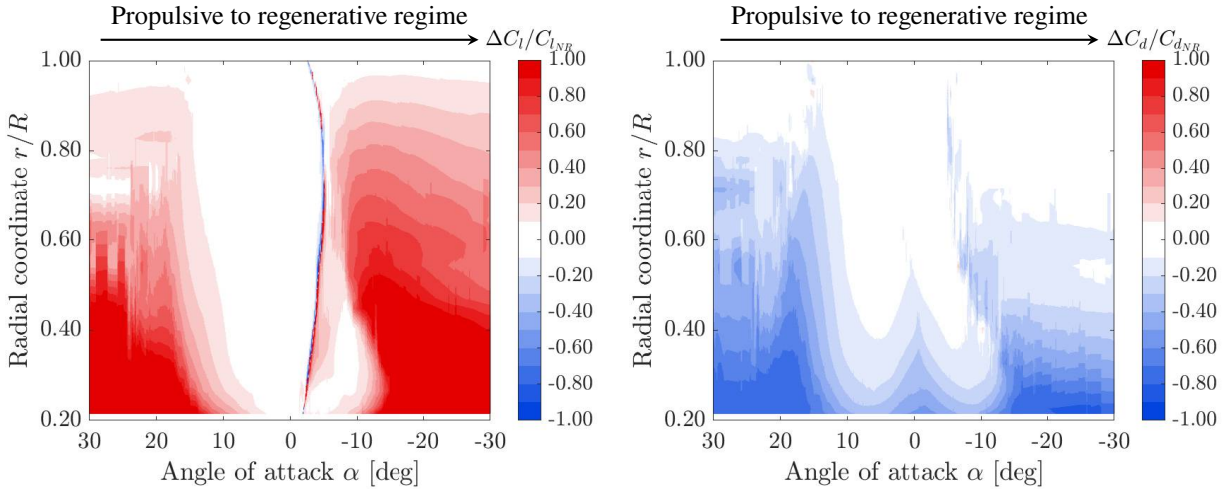

(a) Effect of rotation on sectional lift **(b) Effect of rotation on sectional drag**

Fig. 9 Effect of rotation on sectional characteristics (estimated using RFOIL)

In Figure 9a, the normalized difference between the predicted lift with and without rotational correction is plotted for a representative Reynolds number variation (1×10^5-2×10^5) along the blade span. The red color in the plot means that the lift with rotational correction is overpredicted as compared to the lift without rotational correction. The red-blue line around 0° angle of attack appears due to the normalization when $C_{l_{NR}}$ goes to 0 and provides a clear distinction between propulsive (left side) and regenerative mode (right side). When the blade sections are operating on the left side of the line, there is a considerable range before the rotational correction becomes important. On the other hand, the correction becomes suddenly important upon entering the right side of the line, which is in agreement with the previous observations from Figures 6 and 7. This is a direct consequence of the rapid onset of separation at negative angles of attack.

Similar to the lift, the normalized change in drag is shown in Figure 9b. The blue color in the plot means that the drag with rotational correction is underpredicted as compared to the drag without rotational correction. The large change in drag near 0° angle of attack is due to the very low $C_{d_{NR}}$ values ($C_{d_{NR}} \rightarrow 0$). Now, keeping the $C_{l_{NR}} = 0$ line from Figure 9a in mind, it can be again observed that the rotational correction becomes quickly important upon entering the regenerative regime (right side). Therefore, it can be concluded that for a conventional propeller, the rotational corrections are crucial in the regenerative regime (even at low negative thrust conditions) but are only necessary for the propulsive regime when operating at high blade loading.

C. Blade Loading and Slipstream

Given the flow separation observed in Figure 8, it is necessary to make sure that the BEM model is able to predict the blade loading distribution accurately and not just the integrated forces. However, before comparing the BEM and RANS blade loadings, the radial distribution of average total pressure coefficient obtained from the RANS simulations at 0.2R downstream of propeller center has been compared with the experiment in Figure 10. This comparison helps to evaluate if steady RANS can simulate the slipstream characteristics in the regenerative regime.

Due to the unavailability of experimental data at $J = 0.57$, an additional RANS simulations was carried out at the

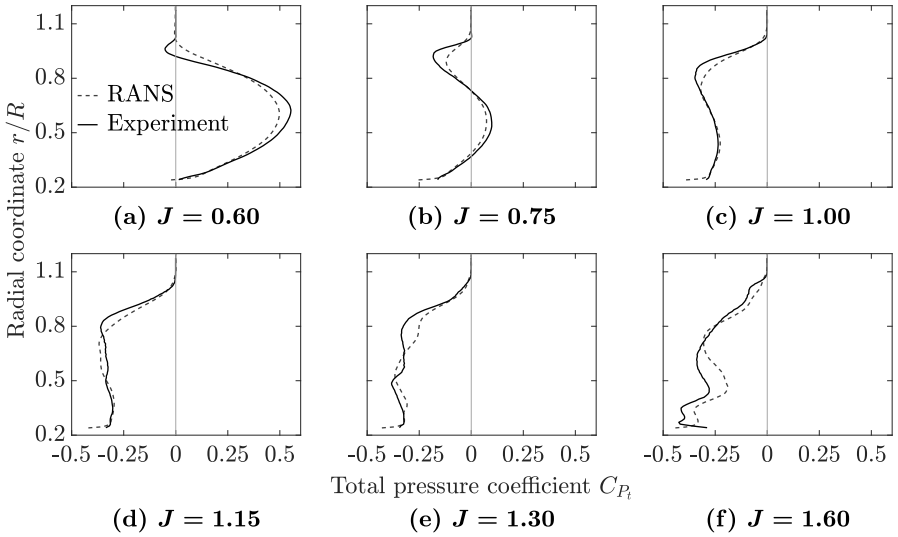

Fig. 10 Total pressure coefficient at 0.2R downstream of propeller center

closest operating condition, i.e., $J = 0.60$ for which the experimental data was available, see Figure 10a. A good match can be observed between the two besides underprediction of the amplitude of C_{P_t} and strong gradients near the tip. RANS is unable to capture the strong gradients due to numerical dissipation. Similar underprediction of the amplitude can also be observed for $J = 0.75$ and 1.00 in Figures 10b and 10c. In Figure 10d, a noticeable difference can be seen between the RANS simulation and the experiment for the outboard part of the blade starting from 0.5R. This difference is enhanced as the advance ratio is increased, however even at higher advance ratios (Figure 10f), a qualitative similarity can be observed between RANS and experiment. As a qualitative reference is sufficient to compare the BEM blade loading, the steady RANS simulations can be considered a good reference for further comparison.

Considering RANS as the reference, a comparison of power and thrust distributions between BEM and RANS is shown in Figures 11 and 12. BEM is in a good agreement with RANS in propulsive mode at $J = 0.57$ (Figures 11a and 12a). At higher advance ratios, both thrust and power are overpredicted by BEM compared to the RANS prediction in the outer part of the blade and are underpredicted in the inner part. The thrust underprediction on the inboard part cancels the outboard overprediction resulting in a similar integrated thrust from BEM and RANS even at higher advance ratios, compare Figures 7a and 11. However, the same is not true for power. The overprediction on the outboard part of

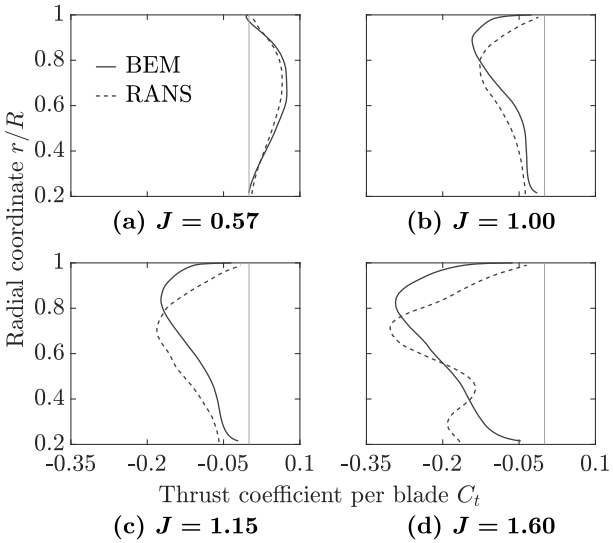

Fig. 11 Thrust distribution along the propeller blade

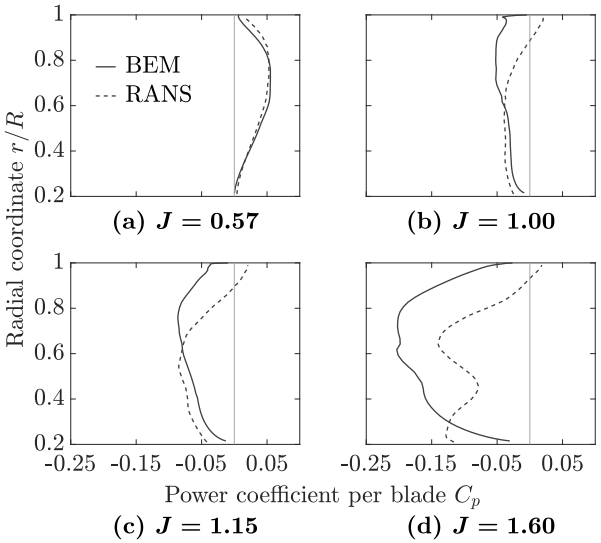

Fig. 12 Power distribution along the propeller blade

the blade is more than the underprediction on the inboard part resulting in a higher integrated power prediction from BEM, compare Figures 7b and 12. At J = 1.60, where the blades are fully stalled as shown with the help of CFD (Figure 8d), the power generation is overpredicted by BEM almost along the whole blade.

The main reason for the overprediction in the outboard region is the delayed stall prediction by RFOIL when the rotational correction model is used, resulting in overpredicted power and thrust in the already stalled regions. Therefore, it can be concluded from the above analysis that the 2-D panel codes, such as XFOIL or RFOIL, are not suitable to capture the blade section characteristics at the negative stall angles of attack faced by the blade sections in the regenerative regime. As a result, the BEM model becomes unsuitable for design optimization studies unless a better source/method is available to obtain accurate polar data for blade sections operating near stall or already stalled conditions. Though a further analysis can be done to validate if momentum theory is applicable at such conditions, it is not necessary for studying the aeroacoustic characteristics of the regenerative regime and is out of the scope of the current study.

D. Sensitivity of Hanson Model to Input Data - BEM Vs RANS

The BEM model overpredicts the blade loading on the outboard part of the blade (Figures 11 and 12). Moreover, it predicts a higher thrust-to-torque ratio (T/Q) for the propulsive regime, whereas a lower thrust-to-torque ratio in the regenerative regime as compared to the RANS simulations (Figure 7). Therefore, it is essential to analyze the sensitivity of Hanson's model to the input loading distribution and T/Q, i.e., their effect on the predicted tonal noise. If

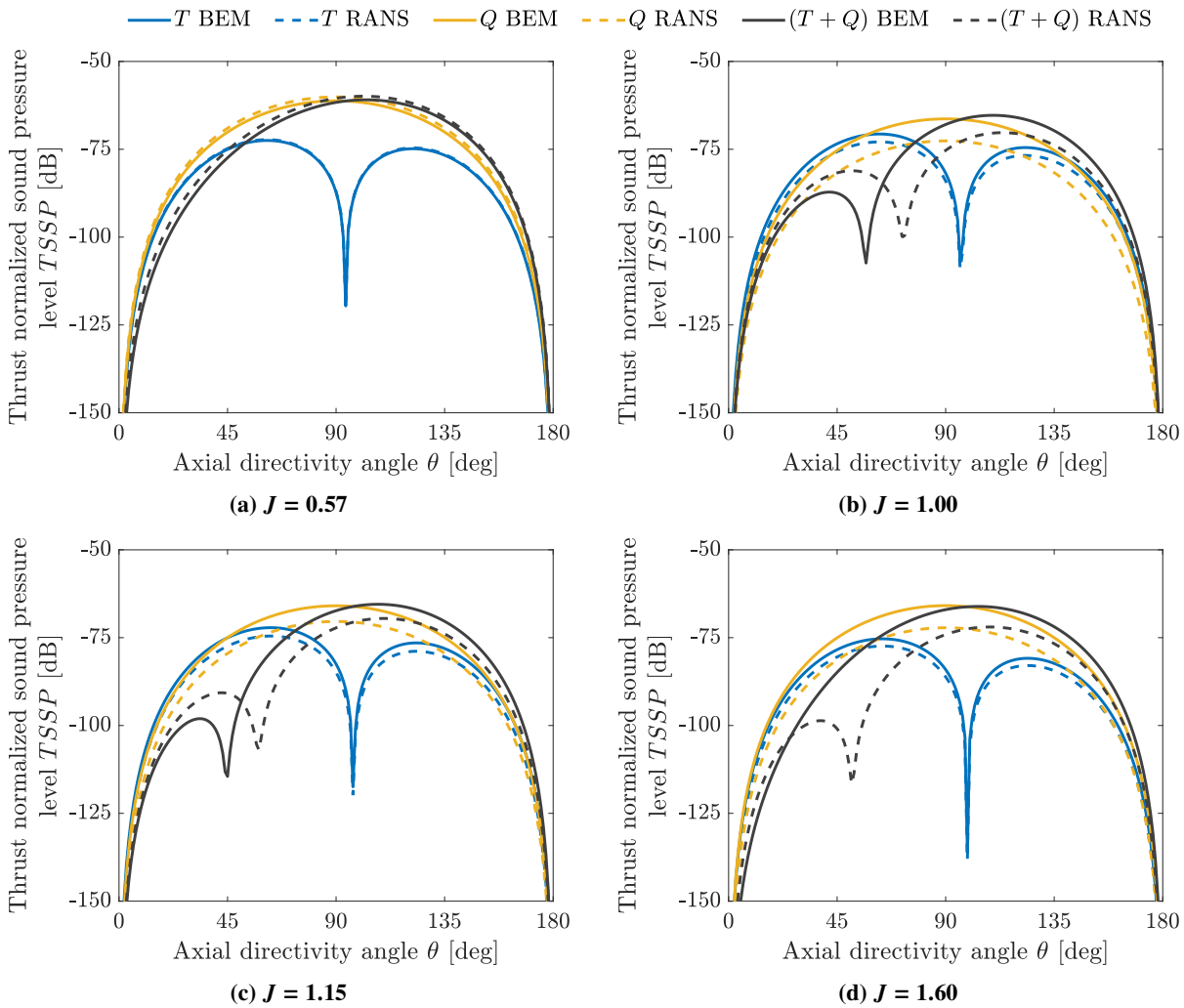

(a) J = 0.57 **(b) J = 1.00**

(c) J = 1.15 **(d) J = 1.60**

Fig. 13 Sensitivity of Hanson's model to the input loading (BEM and RANS)

the resulting differences are small, the BEM model in combination with Hanson's model can be used for tonal noise optimization in the regenerative regime. However, if that is not true, then the RANS simulations need to be used in coupling with Hanson's model.

For a fair comparison between BEM and RANS, the thrust-specific-sound-pressure-level ($TSSP$) has been used to remove any differences due to discrepancies in the integrated thrust value. In $TSSP$, the conventional reference pressure (2×10^{-5} Pa) has been replaced with $\frac{T}{D_p^2}$ [45]:

$$TSSP = 20 \log_{10} \left(\frac{p_{rms}}{\frac{T}{D_p^2}} \right), \tag{1}$$

The loading noise levels computed from the BEM and RANS aerodynamic loadings are compared in Figure 13 at a 10R distance from the propeller. The separate contributions from the thrust (T) and the torque (Q) noise are shown in addition to the sum of the two ($T+Q$). For $J = 0.57$, the normalized thrust and torque noise for BEM and RANS have an excellent agreement which is the direct consequence of the agreement in the blade loading distribution shown previously in Figures 11a and 12a. The 10% overprediction in T/Q by BEM as compared to RANS, results in a 2-3 dB lower thrust normalized loading noise ($T+Q$) predicted using the BEM input in Figure 13a. Hanson's model predicts a considerably higher $TSSP$ for thrust and torque in the regenerative regime for the BEM model as seen in Figures 13b–13d. This is a direct consequence of the higher outboard loading predicted by BEM compared to the RANS results. As the BEM model underpredicts the T/Q by 30%-50% in the regenerative regime as compared to the RANS simulations, it results in a significant difference (5-6 dB) in loading noise ($T+Q$) especially for $J = 1.60$. It is evident from Figure 13 that the torque to thrust ratio plays an important role in the loading noise characteristics. Therefore, RANS coupled with Hanson's model will be used for the further investigation of the aeroacoustic characteristics of the regenerative regime.

Notice that BEM is able to predict the trends in loading noise, i.e., the decrease in the frontal lobe of the loading noise with the increase in advance ratio. Therefore, it can still be used in the regenerative regime with Hanson's model to do a comparative analysis of different operating conditions, and to get an estimate of the trends in the propeller noise emissions with variations in thrust setting.

E. Tonal Noise Characteristics - Positive Vs Negative Thrust

To study the tonal noise characteristics of the isolated propeller in positive and negative thrust conditions, the analysis is carried out for the 6-blade propeller at a constant tip rotational Mach number of 0.62 and freestream Mach number of 0.18 ($J = 0.90$). Keeping the tip rotational Mach number constant decouples the effect of thickness noise from loading noise. The positive and negative thrust conditions are compared at an absolute thrust level, $|T_C| = 0.22$, assuming it to be representative of climb and approach conditions. The aerodynamic loading of the propeller is changed from positive to negative thrust by changing the pitch angle.

Section IV.E.1 describes the setup used to obtain the aerodynamic loading for Hanson's model. The results obtained from Hanson's model to characterize the tonal noise sources in positive and negative thrust conditions are reported in Section IV.E.2.

1. Aerodynamic Performance

Initially, the absolute thrust level was chosen to be $|T_C| = 0.20$. The BEM model was used to find corresponding pitch angles with a sweep from 1° to 50°. The resulting thrust, power coefficients (referenced to freestream dynamic pressure) with pitch angle sweep are shown in Figure 14a. At high pitch angles, the propeller blades operate near positive stall angles resulting in a non-linear trend. By decreasing the pitch angle, the angles of attack at the blade sections decrease, resulting in decreased thrust and power coefficients. A linear trend is observed until the propeller enters the regenerative regime, where a maximum regeneration power is achieved at 11° pitch. A further decrease in the pitch results in decreased power regeneration due to the increased drag in the stalled region. The continued decrease in pitch would lead to a point where power is required to operate the propeller at negative thrust.

The pitch angles corresponding to $T_C = -0.20$ and 0.20 were found to be 11° and 25°, respectively. RANS simulations were performed at these pitch angles to obtain accurate blade loading and T/Q for Hanson's model. At 11° pitch, T_C was found to be -0.22, i.e., 10% higher than the value predicted by BEM. Similarly, for 25° pitch, T_C was 0.17, i.e., 15% lower than the value predicted by BEM. As it is important for the subsequent analysis to compare the tonal characteristics at the same thrust level, the slope of T_C curve from BEM was used to find the pitch corresponding to

T_C = 0.22 for the RANS simulations, i.e., the same magnitude of T_C as obtained by RANS simulations at 11° pitch. This pitch was found to be 26.9 deg, leading to absolute T_C identical up to 4 decimal places.

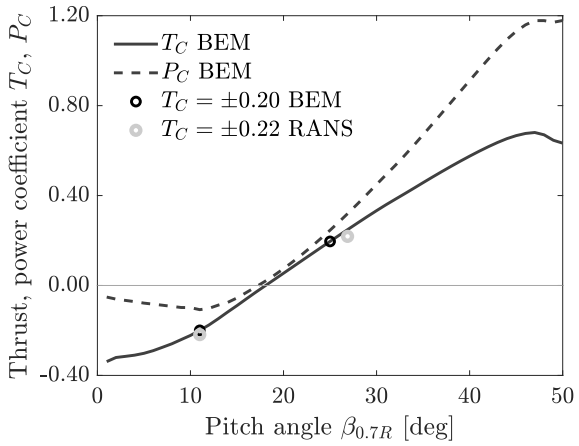

(a) Effect of pitch change on thrust and power coefficient

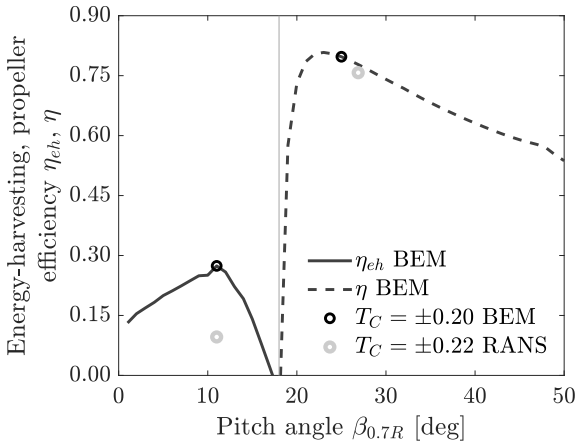

(b) Effect of pitch change on propeller and regenerative efficiency

Fig. 14 Effect of pitch change on propeller performance at J = 0.90

The corresponding energy-harvesting and propeller efficiency for the pitch angle sweep are plotted in Figure 14b. The BEM model predicts a maximum energy-harvesting efficiency of 27% at 11° pitch angle, which is considerably overpredicted as compared to the 10% predicted by RANS. The previously reported values for conventional propellers of around 10-11% are in agreement with the RANS prediction [1, 4]. At 18° pitch, there is a transition from regenerative to the propulsive regime. A maximum propeller efficiency of 81% is predicted at 23° for the selected advance ratio. At higher pitch angles, the angles of attack at the blade sections increase resulting in decreased lift-to-drag ratios, causing a decreased propeller efficiency at the considered operating conditions. At lower rotational speeds, the peak efficiency will occur at higher pitch angles.

The thrust and torque distributions along the blade for 11° and 26.9° pitch angle obtained from RANS simulations are shown in Figure 15. Note that the subsequent aeroacoustic analysis is carried out at $|T_C|$ = 0.22 using these aerodynamic loadings obtained from the RANS simulations. The thrust and torque distributions for the negative thrust case have been plotted with a negative sign to compare the blade loading distribution with the positive thrust case. In the inboard section, the negative thrust condition has higher loading for both thrust and torque, whereas, in the outboard

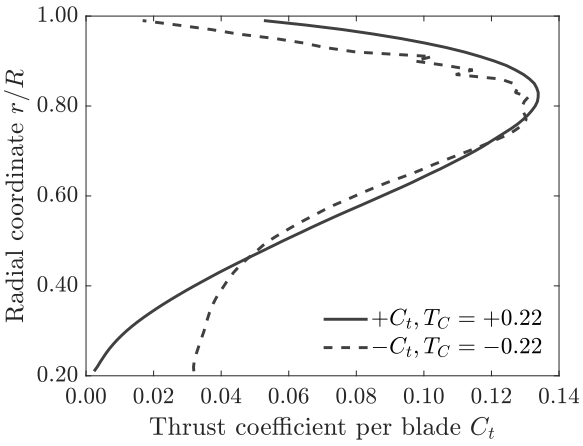

(a) Thrust distribution

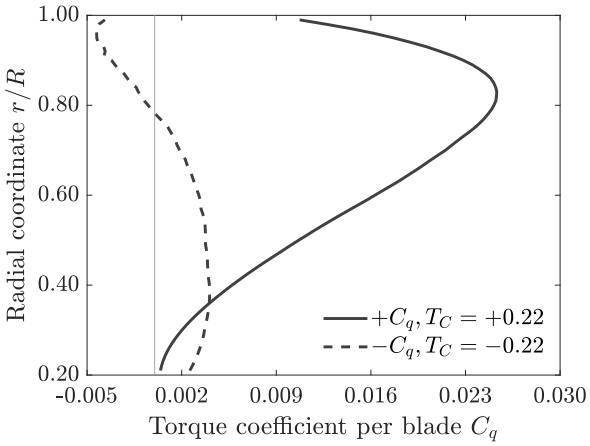

(b) Torque distribution

Fig. 15 Comparison of thrust and torque distribution in propulsive and regenerative regime at T_C = ±0.22, J = 0.90 (RANS data)

section, the thrust loading for the positive thrust case is comparatively higher. The torque loading of the positive thrust case is considerably higher than the negative thrust case except near the root. Twenty percent of the outer blade is completely stalled for the negative thrust case resulting in power dissipation rather than regeneration.

2. Aeroacoustic Performance

The tonal noise can be divided into three sources - thickness noise (monopole), loading noise (dipole), and flow non-linearity noise (quadrupole). In this paper, it is assumed that quadrupole noise can be ignored at the considered operating conditions, i.e., at the subsonic tip rotational Mach number. The loading noise can be further divided into either thrust (T) and torque (Q) noise or lift (L) and drag (D) noise. The comparison of tonal noise directivity for $T_C = \mp 0.22$ at pitch angle of 11.0° and 26.9° is shown in Figure 16.

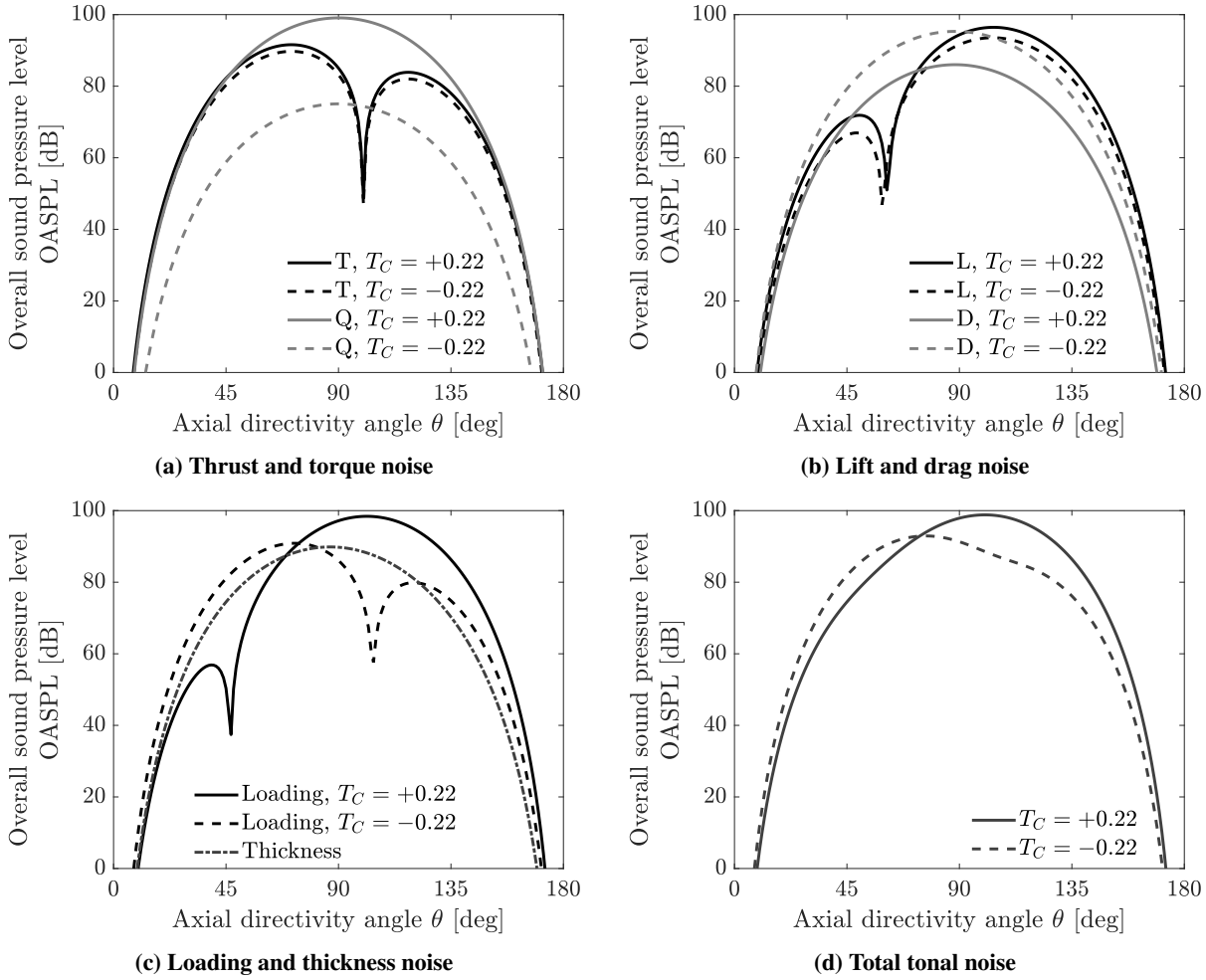

(a) Thrust and torque noise

(b) Lift and drag noise

(c) Loading and thickness noise

(d) Total tonal noise

Fig. 16 Tonal noise directivity at positive and negative thrust, $T_C = \pm 0.22$ and $J = 0.90$ (RANS + Hanson)

The plots show the variation of overall sound pressure level (OASPL) with the axial directivity angle (θ), where OASPL is defined as:

$$\text{OASPL} = 20\log_{10}\left(\frac{\sqrt{\Sigma_m \left(p_{Vm} + p_{Lm} + p_{Dm}\right)^2}}{p_{\text{ref}}}\right) = 20\log_{10}\left(\frac{\sqrt{\Sigma_m \left(p_{Vm} + p_{Tm} + p_{Qm}\right)^2}}{p_{\text{ref}}}\right), \tag{2}$$

where p_{Vm} refers to the pressure fluctuations due to thickness of the blade, p_{Lm} and p_{Dm} refer to pressure fluctuations due to lift and drag, respectively. Similarly, p_{Tm} and p_{Qm} refer to pressure fluctuations due to thrust and torque,

respectively. Note that thrust scaling was not needed in this analysis as the absolute thrust level is the same for the considered cases.

Figure 16a shows the thrust and torque noise directivity. Though the direction of thrust and torque is reversed in the negative thrust case as compared to the positive thrust case, no change is observed in their noise directivity as the resulting pressure fluctuations are unaffected by the direction of the force. Even though the thrust magnitude is the same for both cases, a difference is observed in the thrust noise level. As reported previously in Figure 15a, the positive thrust case has a higher outboard loading resulting in a higher thrust noise than the negative thrust case, even though the integrated thrust values are equal. This trend is expected for conventional propellers due to the stall of the tip in negative thrust cases leading to a lower outboard loading than the positive thrust case.

For the given thrust level at a constant advance ratio, the required torque to generate that thrust will always be higher than the regenerated torque at the same negative thrust level. The reasoning behind this argument is given in Appendix A. Therefore, at a constant advance ratio, the torque noise per unit thrust for the propulsive regime will always be higher than the regenerative regime, which is also exemplified in Figure 16a.

Comparing Figures 16a and 16c, the interference between the thrust and torque stays the same in the positive and the negative thrust case, i.e., destructive interference in the frontal lobe and constructive interference in the backward lobe of the thrust, irrespective of the thrust direction. The reason for no change in the interference pattern is the fact that the torque also changes its direction along with the thrust when going from the propulsive to the regenerative regime, i.e., the sign of thrust and torque stays the same in both the regimes. This assertion has been verified by analyzing the loading noise near the transition from propulsive to the regenerative regime, i.e., $\beta_{0.7R} = 18°$ at which the thrust and the torque have opposite signs (Figure 14a). At this operating condition, the thrust is already negative (T_C = -0.0021), whereas the power required is positive (P_C = 0.0181). The loading noise along with its thrust and torque contributions has been shown in Figure 17.

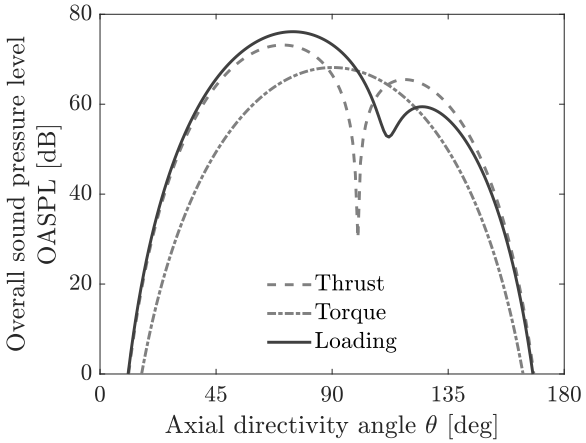

Fig. 17 Loading noise contribution at the transition from propulsive to regenerative regime $J = 0.90$, $\beta_{0.7R} = 18°$, $T_C = -0.0021$, $P_C = 0.0181$ (BEM + Hanson)

Note that in contrast to the conventional case (in which thrust and torque have the same sign) [46], the frontal lobe of the thrust noise interferes constructively with the torque noise and the backward lobe interferes destructively. Therefore, when the thrust and the torque have the same sign, i.e., the torque is in 90° phase lead of the thrust (positive in the counter-clockwise direction), there is destructive interference between the frontal lobe of the thrust noise and the torque noise. In addition, constructive interference occurs between the backward lobe of the thrust noise and the torque noise. However, when the thrust and the torque have the opposite sign, i.e., the torque is in 90° phase lag of the thrust, the interference is reversed.

The corresponding lift and drag noise decomposition is shown in Figure 16b. Again, the directivity of the lift noise is not affected when changing from the positive to the negative thrust case, though the direction of the lift is reversed. It has been proven in Appendix A that at a given advance ratio, the lift force in the positive thrust case will always be higher than the equally negative thrust case. Therefore, the lift noise in the propulsive regime will always be higher than in the regenerative regime, also reflected in Figure 16b. As the propeller blade operates in stalled conditions in the regenerative regime, the drag force is much higher in the regenerative case than in the propulsive case. Therefore, for a conventional propeller, the tonal drag noise for negative thrust will always be higher than for the equal but positive

thrust, also exemplified by Figure 16b. Moreover, as the direction of the lift force reverses between the two regimes and the drag force direction stays the same, the phase difference between the lift and the drag force is changed by 180° between the two regimes. This change in the phase difference results in an opposite interference between these two noise-generating mechanisms for the two modes of propeller operation. For the propulsive regime, the frontal lobe of the lift noise interferes destructively with the drag noise and the backward lobe interferes constructively, as evident from the reduced frontal lobe of the loading noise in Figure 16c. In the regenerative regime, this interference behavior is reversed, leading to a more dominant frontal lobe in the loading noise.

Figure 16c shows the loading noise directivity for the given positive and negative thrust along with the thickness noise. As the tip Mach number is constant, the thickness noise is the same for both conditions. A dominant forward directivity and a decreased backward noise level are observed for the regenerative regime compared to its counter case at the given advance ratio of $J = 0.90$. Given the two observations from the above analysis -

1) for a given absolute thrust level at a given advance ratio, a lower torque noise, and a slightly lower thrust noise is expected for the regenerative regime than for the propulsive regime;
2) the frontal lobe of the thrust noise interferes destructively with the torque noise and the backward lobe interferes constructively in both regimes (given that thrust and torque have the same sign in the propulsive as well as the regenerative regime);

it can be concluded that downstream of the propeller, the regenerative regime will always have a lower loading noise as compared to the propulsive case. As for the upstream directivity, it is dependent on the comparative level of the thrust

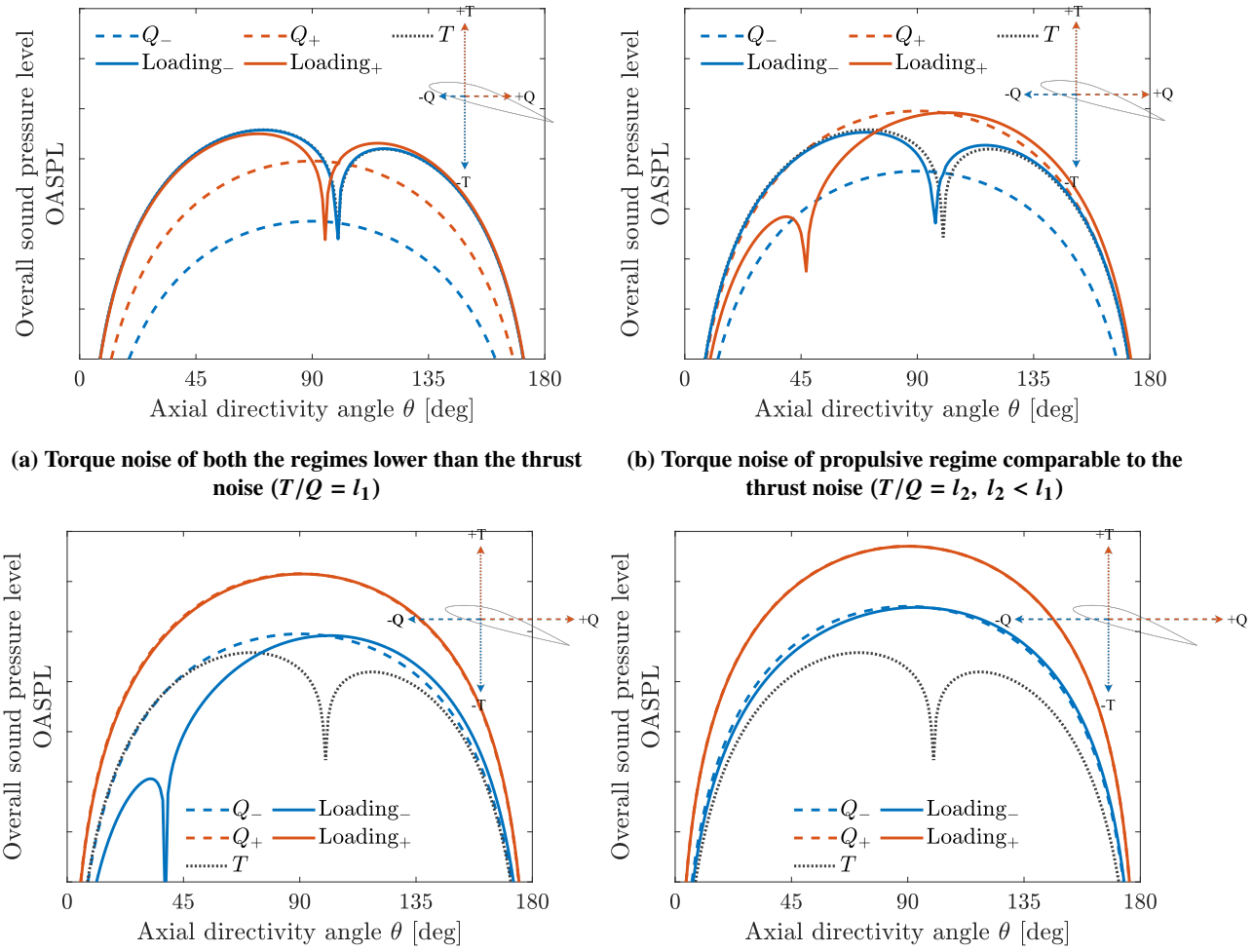

(a) Torque noise of both the regimes lower than the thrust noise ($T/Q = l_1$)

(b) Torque noise of propulsive regime comparable to the thrust noise ($T/Q = l_2,\ l_2 < l_1$)

(c) Torque noise of regenerative regime comparable to the thrust noise ($T/Q = l_3,\ l_3 < l_2$)

(d) Torque noise of both the regimes higher than the thrust noise ($T/Q = l_4,\ l_4 < l_3$)

Fig. 18 Illustration of the effect of thrust-to-torque ratio (T/Q) on loading noise directivity at a given thrust

and torque noise which in turn is dependent on the thrust-to-torque ratio (T/Q). Four different scenarios are possible (assuming thrust noise of both regimes is equal), see Figure 18.

The first case (Figure 18a) is possible at extremely low advance ratios, where the thrust-to-torque ratio has a high value (let $T/Q = l_1$) so that the torque noise of both regimes is lower than the thrust noise. In such a scenario, the thrust noise becomes the dominant source of tonal loading noise. If the M_{tip} is increased to reach the low advance ratio, the thickness noise might also become an important source. However, as the thrust noise and M_{tip} are assumed to be the same for both the regimes, therefore, in this case, the overall loading noise (Figure 18a) and the thickness noise will be similar for both the regimes. Therefore, the tonal noise in such a scenario will not depend significantly upon the mode of operation.

The second case (Figure 18b) represents a comparatively lower thrust-to-torque ratio (let $T/Q = l_2$) than the first case, i.e. $l_2 < l_1$. The value of T/Q is taken such that the propulsive torque noise is comparable to the thrust noise. Such a scenario is expected to occur at a relatively higher advance ratio than the first case. An example of the second scenario is the condition discussed above in Figure 16 and could be relevant for climb and approach conditions. In such a scenario, the regenerative regime will have a dominant forward directivity and decreased backward loading noise as compared to the propulsive regime, see Figure 18b. However, the thickness noise might also be relevant at such conditions which could mitigate the dominant forward directivity of loading noise to some extent, as seen before in Figure 16d.

Figure 18c describes a scenario with $T/Q = l_3$ so that $l_3 < l_2$. The value of T/Q is taken such that the corresponding regenerative torque noise is comparable to the thrust noise, whereas the propulsive torque noise is higher than the thrust noise. The propulsive loading noise will be dominated by the torque noise and the frontal lobe will be eliminated. On the other hand, the forward directivity of the regenerative regime will be diminished due to destructive interference between the thrust and the torque noise as shown in Figure 18c. Such a scenario is expected to occur at higher advance ratios than the previous two cases. If the negative thrust mode of the propeller is to be used just as an additional drag device rather than for regeneration, this scenario could be useful due to its reduced loading noise, and therefore, reduced landing/approach noise. However, the thickness noise might mitigate the effect of decreased forward loading noise to some extent. Moreover, the broadband noise could become important in this scenario due to the significant separation of the flow over the blades.

The last case (Figure 18d) refers to the situation with the lowest T/Q as compared to the previous scenarios so that the torque noise for both regimes is higher than the thrust noise. As in this case the torque noise will be dominant, the loading noise of the regenerative regime will be lower than the propulsive regime. This case is expected to occur at higher advance ratios than the rest of the scenarios.

V. Conclusions

In this study, the applicability of the low-fidelity BEM model and the RANS simulations for the prediction of propeller performance at positive and negative thrust has been investigated by comparison against experimental data. Using these aerodynamic tools (BEM and RANS) in coupling with Hanson's model, the tonal noise characteristics of the less explored regenerative regime have been studied in comparison with the well-known propulsive regime.

The following conclusions are drawn about the accuracy of BEM and RANS in the regenerative regime:

- The BEM model without correction for rotational effects is not suitable for regenerative performance prediction.
- The inclusion of rotational effects in polar data improves the integrated performance prediction of BEM in regenerative conditions. Though BEM can predict the integrated thrust even at high advance ratios, it overpredicts the regenerated power and cannot be used after a certain advance ratio (due to significant flow separation) for power prediction.
- Though BEM can predict the integrated thrust value, the predicted blade loading distributions tend to underpredict the loading for inboard sections and overpredict for the outboard sections. The same is true for power distribution. The main reason for this overprediction is the delay in the stall prediction in the polar data.
- The inaccurate blade loading prediction makes the BEM model unsuitable for design optimization studies focused on the improvement of regenerative performance unless a better source/method is available to obtain accurate polar data for the blade sections at negative angles of attack (near stall or in already stalled conditions).
- The RANS simulations provide an excellent agreement with the experimental integrated performance data up to operating conditions with significant flow separation. However, in conditions with complete flow separation on the blades, RANS provide a conservative estimation of thrust and power, as compared to the experiment.
- Slipstream total pressure predicted by RANS is in good qualitative agreement with the experimental data even for

operating conditions with complete flow separation on the blades.

The far-field aeroacoustic tonal noise characteristics of the propeller in the regenerative regime have been studied in comparison with the conventional propulsive regime at a constant tip Mach number and freestream Mach number using Hanson's frequency-domain model. The following conclusions are drawn:

- The sensitivity analysis shows that despite the inaccurate blade loading predictions, BEM can be coupled with Hanson's model to do a comparative analysis of the propeller noise emissions in different operating conditions.
- The change in thrust and torque direction does not affect the associated noise directivity and noise levels individually.
- As the propulsive regime is always expected to have a higher outboard loading compared to the regenerative regime (due to the stall of the tip in the latter case), a higher thrust noise is expected in the propulsive regime at a given absolute thrust level.
- For a given thrust at a constant advance ratio, the required torque to generate that thrust will always be higher than the regenerated torque at the same absolute thrust level in regenerative conditions. Therefore, at a given advance ratio, the torque noise per unit thrust for the propulsive regime will always be higher than for the regenerative regime.
- The interference between two noise-generating mechanisms (for example - lift and drag, or thrust and torque) stays the same as long as the phase difference between the mechanisms is maintained, irrespective of the propulsive or regenerative regime. If the phase difference is reversed, the interference is reversed as well.
- At a constant advance ratio and a constant absolute thrust level, the lift in the propulsive case is always higher than in the regenerative regime, resulting in a higher lift noise in the propulsive regime.
- As the drag in the regenerative regime is expected to be higher than the propulsive regime due to stall of the blade sections in the former, the drag noise in the former is expected to be higher than in the latter.
- Downstream of the propeller, the loading noise in regenerative conditions is always lower than in propulsive conditions. The loading noise upstream of the propeller depends on the relative level of thrust and torque noise, i.e., thrust-to-torque ratio.

The results presented in this paper enhance the understanding of the aerodynamic and aeroacoustic performance of isolated propellers at positive and negative thrust settings. The investigations into the performance at negative thrust may be especially relevant for future electric flight. The follow-up work will focus on a comparison of the broadband noise emissions in both regimes.

Appendix A

The thrust and torque at a blade section in both regimes can be given as (refer to Figure 1):

$$C_{t_+} = C_{l_+} \cos\phi - C_{d_+} \sin\phi\,, \tag{3}$$

$$C_{t_-} = C_{l_-} \cos\phi + C_{d_-} \sin\phi\,, \tag{4}$$

$$C_{q_+} = r \cdot \left(C_{l_+} \sin\phi + C_{d_+} \cos\phi\right)\,, \tag{5}$$

$$C_{q_-} = r \cdot \left(C_{l_-} \sin\phi - C_{d_-} \cos\phi\right)\,, \tag{6}$$

where C_t, C_q are the thrust and torque coefficients, respectively, experienced by the blade section for a given inflow angle ϕ. C_l and C_d represent the corresponding lift and drag coefficients, respectively. r represents the radial location along the blade. The subscript '+' refers to the propulsive case, and '−' refers to the regenerative case. The forces in the propulsive and the regenerative regime are taken positive in opposite directions. As in the following analysis, the rotational and freestream velocities are assumed constant and only pitch is varied to switch from positive to negative thrust, ϕ can be assumed to be constant ignoring the induction.

For the current analysis, as thrust is kept constant ($T_C = \pm 0.22$), therefore, by equating Eq. (3) and (4), $\tan\phi = \frac{C_{l_+} - C_{l_-}}{C_{d_+} + C_{d_-}}$ is obtained. As $\phi \in (0°, 90°)$, it can be concluded that $C_{l_+} > C_{l_-}$ and subsequently by comparing Eq. (5) and (6), it is proven that $C_{q_+} > C_{q_-}$ as given in Eq. (7).

$$\tan\phi = \frac{C_{l_+} - C_{l_-}}{C_{d_+} + C_{d_-}} \implies C_{l_+} > C_{l_-} \implies C_{q_+} > C_{q_-}\,, \quad \phi \in (0°, 90°)\,. \tag{7}$$

Acknowledgments

The research leading to these results is part of the FUTPRINT50 project. This project has received funding from the European Union's Horizon 2020 Research and Innovation programme under Grant Agreement No 875551. Additionally, the authors would like to acknowledge the contribution of Nando van Arnhem and Tom Stokkermans to the validation experiments for the propulsive condition.

References

[1] Sinnige, T., Stokkermans, T. C. A., van Arnhem, N., and Veldhuis, L. L. M., "Aerodynamic Performance of a Wingtip-Mounted Tractor Propeller Configuration in Windmilling and Energy-Harvesting Conditions," *AIAA Aviation 2019 Forum*, AIAA Paper 2019-3033, June 2019. https://doi.org/10.2514/6.2019-3033.

[2] Eržen, D., Andrejašič, M., Lapuh, R., Tomažič, J., Gorup, Č., and Kosel, T., "An Optimal Propeller Design for In-Flight Power Recuperation on an Electric Aircraft," *2018 Aviation Technology, Integration, and Operations Conference*, AIAA Paper 2018-3206, June 2018. https://doi.org/10.2514/6.2018-3206.

[3] Gunnarsson, G., Skúlason, J. B., Sigurbjarnarson, A., and Enge, S., "Regenerative Electric/Hybrid Drive Train for Ships," Nordic Innovation Publication 2016:02, Jan. 2016.

[4] Nodama, T., and Sunada, S., "Puropera ni yoru batteri jūden ni kansuru kentō [A Study on battery charging by propellers]," *Proceedings of the Japan Society for Aeronautics and Astronautics*, Vol. 63, No. 1, 2015, pp. 8–12. https://doi.org/10.2322/jjsass.63.8.

[5] Hartman, E. P., "Negative Thrust and Torque Characteristics of an Adjustable-pitch Metal Propeller," *Annual Report-National Advisory Committee for Aeronautics*, Vol. 19, 1933, p. 421. URL http://hdl.handle.net/2060/19930091538.

[6] Hedrick, W. S., and Douglass, W. M., "An Experimental Investigation of the Thrust and Torque Produced by Propellers Used as Aerodynamic Brakes," Tech. Rep. NACA-WR-A-27, National Advisory Committee for Aeronautics, 1944. URL http://hdl.handle.net/2060/19930093338.

[7] MacCready, P. B., "Regenerative Battery-Augmented Soaring," *Technical Soaring*, Vol. 23, No. 1, 1999, pp. 28–32.

[8] Barnes, J. P., "Flight Without Fuel – Regenerative Soaring Feasibility," *General Aviation Technology Conference and Exhibition*, SAE Technical Paper 2006-01-2422, Aug. 2006. https://doi.org/10.4271/2006-01-2422.

[9] Galvão, F. L., "A Note on Glider Electric Propulsion," *Technical Soaring*, Vol. 36, No. 4, 2012, pp. 94–101.

[10] Barnes, J. P., "Regenerative Electric Flight: Synergy and Integration of Dual-Role Machines," *53rd AIAA Aerospace Sciences Meeting*, AIAA Paper 2015-1302, Jan. 2015. https://doi.org/10.2514/6.2015-1302.

[11] Courty-Audren, S., Binder, N., Carbonneau, X., and Challas, F., "Potential of Power Recovery of an Axial Fan in Windmilling Operation," *10th European Turbomachinery Conference*, Apr. 2010.

[12] Gill, A., Von Backström, T. W., and Harms, T. M., "Flow Fields in an Axial Flow Compressor During Four-Quadrant Operation," *Journal of Turbomachinery*, Vol. 136, No. 6, 2014. https://doi.org/10.1115/1.4025594.

[13] García Rosa, N., Dufour, G., Barènes, R., and Lavergne, G., "Experimental Analysis of the Global Performance and the Flow Through a High-Bypass Turbofan in Windmilling Conditions," *Journal of Turbomachinery*, Vol. 137, No. 5, 2015. https://doi.org/10.1115/1.4028647.

[14] Binder, N., Courty-Audren, S.-K., Duplaa, S., Dufour, G., and Carbonneau, X., "Theoretical Analysis of the Aerodynamics of Low-Speed Fans in Free and Load-Controlled Windmilling Operation," *Journal of Turbomachinery*, Vol. 137, No. 10, 2015. https://doi.org/10.1115/1.4030308.

[15] Ortolan, A., Courty-Audren, S.-K., Binder, N., Carbonneau, X., García Rosa, N., and Challas, F., "Experimental and Numerical Flow Analysis of Low-Speed Fans at Highly Loaded Windmilling Conditions," *Journal of Turbomachinery*, Vol. 139, No. 7, 2017. https://doi.org/10.1115/1.4035656.

[16] Thomas, J. L., and Hansman, R. J., "Community Noise Reduction Assessment of Using Windmilling Drag on Approach by Hybrid Electric Aircraft," *AIAA Aviation 2020 Forum*, AIAA Paper 2020-2877, June 2020. https://doi.org/10.2514/6.2020-2877.

[17] Hanson, D. B., "Helicoidal surface theory for harmonic noise of propellers in the far field," *AIAA Journal*, Vol. 18, No. 10, 1980, pp. 1213–1220. https://doi.org/10.2514/3.50873.

[18] Sinnige, T., van Arnhem, N., Stokkermans, T. C. A., de Vries, R., van der Beek, B., Jarlstrom, H., Hoogreef, M. F. M., and Veldhuis, L. L. M., "Aerodynamic Analysis of Propellers in Propulsive and Regenerative Conditions," *AIAA Aviation 2020 Forum (oral presentation)*, 2020.

[19] Sinnige, T., "Aerodynamic and Aeroacoustic Interaction Effects for Tip-Mounted Propellers: An Experimental Study," Ph.D. thesis, Delft University of Technology, Sep. 2018. https://doi.org/10.4233/uuid:214e1e9a-c53e-47c7-a12c-b1eb3ec8293b.

[20] Li, Q., Öztürk, K., Sinnige, T., Ragni, D., Eitelberg, G., Veldhuis, L., and Wang, Y., "Design and Experimental Validation of Swirl-Recovery Vanes for Propeller Propulsion Systems," *AIAA Journal*, Vol. 56, No. 12, 2018, pp. 4719–4729. https://doi.org/10.2514/1.J057113.

[21] Stokkermans, T. C. A., and Veldhuis, L. L. M., "Propeller Performance at Large Angle of Attack Applicable to Compound Helicopters," *AIAA Journal*, Vol. 59, No. 6, 2021, pp. 2183–2199. https://doi.org/10.2514/1.J059509.

[22] Rwigema, M. K., "Propeller Blade Element Momentum Theory with Vortex Wake Deflection," *27th International congress of the aeronautical sciences*, ICAS Paper 2010-2.3.3, 2010. URL http://www.icas.org/ICAS_ARCHIVE/ICAS2010/PAPERS/434.PDF.

[23] Burton, T., Sharpe, D., Jenkins, N., and Bossanyi, E., *Wind energy handbook*, Vol. 2, Wiley Online Library, 2001. https://doi.org/10.1002/9781119992714.

[24] van Rooij, R., "Modification of the boundary layer calculation in RFOIL for improved airfoil stall prediction," Report IW-96087R Delft University of Technology, the Netherlands, Sep. 1996.

[25] Drela, M., "XFOIL: An Analysis and Design System for Low Reynolds Number Airfoils," *Low Reynolds Number Aerodynamics*, edited by T. J. Mueller, Springer Berlin Heidelberg, Berlin, Heidelberg, 1989, pp. 1–12.

[26] Yu, W., Zhang, M. M., and Xu, J. Z., "Effect of smart rotor control using a deformable trailing edge flap on load reduction under normal and extreme turbulence," *Energies*, Vol. 5, No. 9, 2012, pp. 3608–3626. https://doi.org/10.3390/en5093608.

[27] Snel, H., Houwink, R., and Bosschers, J., "Sectional Prediction of Lift Coefficients on Rotating Wind Turbine Blades in Stall," Report ECN-93-052, Energy Research Center of the Netherlands, Petten, the Netherlands., 1993.

[28] Bosschers, J., Montgomerie, B., Brand, A., and van Rooij, R., "Influence of Blade Rotation on the Sectional Aerodynamics of Rotational Blades," *22nd European Rotorcraft Forum, England*, 1996.

[29] Anon., "ANSYS® Academic Research Release 2019 R3 Help System, Fluent," ANSYS, inc., Canonsburg, PA, 2019.

[30] Stokkermans, T. C. A., van Arnhem, N., Sinnige, T., and Veldhuis, L. L. M., "Validation and Comparison of RANS Propeller Modeling Methods for Tip-Mounted Applications," *AIAA Journal*, Vol. 57, No. 2, 2019, pp. 566–580. https://doi.org/10.2514/1.J057398.

[31] van Arnhem, N., Vos, R., and Veldhuis, L. L. M., "Aerodynamic Loads on an Aft-Mounted Propeller Induced by the Wing Wake," *AIAA Scitech 2019 Forum*, AIAA Paper 2019-1093, Jan. 2019. https://doi.org/10.2514/6.2019-1093.

[32] Spalart, P. R., and Allmaras, S. R., "A One-Equation Turbulence Model for Aerodynamic Flows," *30th Aerospace Sciences Meeting*, AIAA Paper 1992-439, June 1992. https://doi.org/10.2514/6.1992-439.

[33] Dacles-Mariani, J., Zilliac, G. G., Chow, J. S., and Bradshaw, P., "Numerical/Experimental Study of a Wingtip Vortex in the Near Field," *AIAA Journal*, Vol. 33, No. 9, 1995, pp. 1561–1568. https://doi.org/10.2514/3.12826.

[34] Roache, P. J., "Quantification of Uncertainty in Computational Fluid Dynamics," *Annual Review of Fluid Mechanics*, Vol. 29, No. 1, 1997, pp. 123–160. https://doi.org/10.1146/annurev.fluid.29.1.123.

[35] Eça, L., and Hoekstra, M., "Discretization Uncertainty Estimation Based on a Least Squares Version of the Grid Convergence Index," *Proceedings of the Second Workshop on CFD Uncertainty Analysis*, 2006.

[36] Gutin, L., "On the Sound Field of a Rotating Propeller," Tech. Rep. NACA-TM-1195, National Advisory Committee for Aeronautics, 1948. URL http://hdl.handle.net/2060/20030068996.

[37] Demming, A. F., "Noise from propellers with symmetrical sections at zero blade angle," Tech. Rep. NACA-TN-605, National Advisory Committee for Aeronautics, 1937. URL http://hdl.handle.net/2060/19930081380.

[38] Barry, F. W., and Magliozzi, B., "Noise detectability prediction method for low tip speed propellers," Tech. Rep. AFAP:-TR-71-37, Air Force Aero Propulsion Laboratory, June 1971.

[39] Farassat, F., and Succi, G. P., "The prediction of helicopter rotor discrete frequency noise," *American Helicopter Society*, Jan. 1982, pp. 497–507. URL https://ui.adsabs.harvard.edu/abs/1982ahs..proc..497F.

[40] Kotwicz Herniczek, M. T., Feszty, D., Meslioui, S.-A., Park, J., and Nitzsche, F., "Evaluation of acoustic frequency methods for the prediction of propeller noise," *AIAA Journal*, Vol. 57, No. 6, 2019, pp. 2465–2478. https://doi.org/10.2514/1.J056658.

[41] Soderman, P., Horne, W., and Center, A. R., "Acoustic and Aerodynamic Study of a Pusher-propeller Aircraft Model," *NASA technical paper 3040*, 1990.

[42] Szydlowski, J., and Costes, M., "Simulation of Flow Around a Static and Oscillating in Pitch NACA 0015 Airfoil Using URANS and DES," *Heat Transfer Summer Conference*, Vol. 2, Parts A and B, July 2004, pp. 891–908. https://doi.org/10.1115/HT-FED2004-56437.

[43] Shelton, A., Abras, J., Jurenko, R., and Smith, M., "Improving the CFD Predictions of Airfoils in Stall," *43rd AIAA Aerospace Sciences Meeting and Exhibit*, AIAA Paper 2005-1227, 2005. https://doi.org/10.2514/6.2005-1227.

[44] Himmelskamp, H., *Profile Investigations on a Rotating Airscrew*, Ph.D. Dissertation, Gottingen, Germany, 1945.

[45] Geng, X., Hu, T., Liu, P., Sinnige, T., and Eitelberg, G., "Analysis of Thrust-Scaled Acoustic Emissions of Aircraft Propellers and Their Dependence on Propulsive Efficiency," *ICAS Paper 2020-0751*, 2021.

[46] Kurtz, D., and Marte, J., "A review of aerodynamic noise from propellers, rotors, and lift fans," Tech. Rep. 32-1462, Jet Propulsion Laboratory, Jan. 1970.